ACS OMEGA

Open Access

http://pubs.acs.org/journal/acsodf

Article

Proteome Analysis of the ROF-FKBP Mutants Reveals Functional Relations among Heat Stress Responses, Plant Development, and Protein Quality Control during Heat Acclimation in *Arabidopsis thaliana*

Paraskevi Lefa, Martina Samiotaki, and Theodora Farmaki*

Cite This: *ACS Omega* 2024, 9, 2391−2408

Read Online

ACCESS | Metrics & More | Article Recommendations | Supporting Information

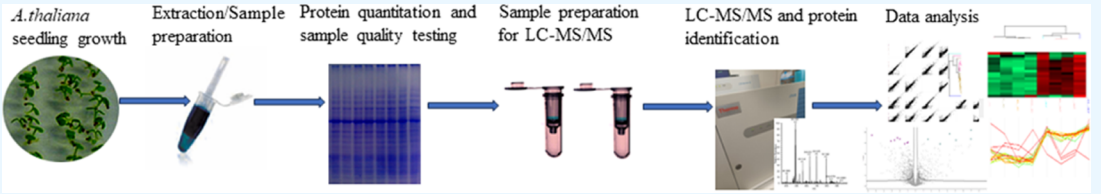

ABSTRACT: In the present study, a differential screening following heat stress acclimation was performed in *Arabidopsis thaliana* WT and ROF-FKBP mutated plants using mass spectrometry, and the results were used to understand and analyze the effect of the ROF PPIases during thermotolerance acquisition in plants. Our data highlight the central role of these two PPIases in heat stress and point to their direct or indirect effect on other proteins participating in cellular functions such as protein folding and quality control, cell division, photosynthesis, and other metabolic and signaling processes. Specifically, the heat stress response, protein folding, and protein ER processing pathways are enhanced following a 37 °C acclimation period independent of the mutation state. However, at 37 °C, and in the double-mutated *rof1*$^{-}$/2^{-} plants, a higher accumulation of proteins belonging to the above pathways is observed compared with all other conditions (WT, single mutants, control, and heat-acclimated plants). Furthermore, the proteasomal pathway, involving the common member of both the protasomal and the lysosomal degradation pathway, CDC48, is over-represented in the extracts of both the untreated and heat-stressed *rof1*$^{-}$/2^{-} mutants compared with the other extracts. In contrast, in the single *rof1*$^{-}$ mutation, the heat acclimation pathway is suppressed at 37 °C when compared to the WT. Protein accumulation related to the heat stress and the protein quality control pathways points to a differential but also synergistic role of the two proteins. Protein complexes of other biochemical and developmental mechanisms, such as the light-harvesting complex of the photosynthetic pathway and the phosphoinositide binding proteins involved in membrane-trafficking events during cell plate formation and cytokinesis (patellin 1, 2, and 4), are negatively regulated in the *rof1*$^{-}$/2^{-} mutant. Our results suggest that ROF1 and ROF2 FKBPs regulate stress response, and developmental and metabolic pathways via a complex feedback mechanism involving partners that ensure protein quality control and plant survival during heat stress.

1. INTRODUCTION

Several plant species adapt to increasing temperature via a process called heat acclimation. Heat acclimation involves biochemical and structural changes that facilitate the plant's ability to face high lethal temperatures. During this process, plants are exposed to sublethal temperatures for a certain period, allowing the formation of functional and structural components that bring resistance to the new adverse environment. Genome and proteome responses to heat stress have been extensively studied.[1] However, there is limited knowledge regarding proteome changes and their functional implications during heat acclimation in relation to the key regulators of developmental and growth processes.

Heat stress impedes normal cellular functions via its direct or indirect protein denaturation effect. A central role in heat stress response (HSR) is played by the heat-induced chaperones, heat shock proteins (HSPs).[2] Chaperone recruitment, involved in protein folding, prevention of protein misfolding and aggregation, and in the regulation of proper protein function, translocation, and degradation,[3] ensures plant functional and, consequently, phenotypic stability. Furthermore, protein misfolding results in ROS production, causing severe damage to nucleotides and membranes and resulting in cell death,[3] a fact that places the heat-related chaperones in a central position in the development of the heat stress resistance mechanism and the

Received: September 7, 2023
Revised: November 24, 2023
Accepted: December 7, 2023
Published: December 26, 2023

consequent plant survival. Together with the heat-perceiving calcium channels, they secure plasma membrane structural integrity and stability.[4] On the other hand, ROS act as second messengers in mammalian systems and plants, and a direct impact of H_2O_2 on chaperones has been shown.[5]

During the daily temperature fluctuation, plants accumulate protective enzymes and metabolites such as HSPs, carotenoids, glutathione, proline, and trehalose.[6] Following an acute heat wave, massive protein misfolding and aggregation cause blocking of the chaperone function and, together with the other deleterious effects of heat, may cause system breakdown. However, a moderate increase in the environmental temperature, prior to a lethal heat attack, induces massive chaperone transcription and accumulation.

HSPs are divided into six main classes: HSP20s, HSP60s, HSP70-HSP110, HSP90, HSP100, and HSP40. HSP20s are ubiquitous proteins and the main chaperone family in plants. They respond to heat stress following a massive expression from a null basal level.[7] They were suggested to collaborate with other HSPs (70, 40, 60, and 100) in the refolding of denatured proteins,[8] protect membranes during heat stress, and repress heat-induced apoptosis.[8] In contrast, HSP70s are constitutively expressed, with some of them being strongly upregulated by heat stress.[9] Using energy from ATP hydrolysis, they coordinate cellular proteostasis by remodeling stress misfolded proteins with the codisaggregation action of the also constitutively expressed HSP100s and the catalytic action of HSP40s and DNAJs (JDPs). HSP90s are also heat stress-inducible chaperones, which apart from their HSFA1 regulatory property,[10] in combination with HSP70s, ensure proper and complete protein folding.

Through a cascade of interactions and modifications, chaperones enter the nucleus, wherefrom they regulate the HSR gene expression.[11] HSPs are transcriptionally controlled by the HSFs (heat shock factors) belonging to three classes A, B, and C. Together with the HSPs, they define the acclimation level of the organism both quantitatively and qualitatively. Class A HFSs triggering HSR and class B HSFs have been shown to participate in the recovery from heat stress.[12] In *Arabidopsis*, HSFA1 isoforms are constitutively expressed, maintain a basal thermotolerance, and initiate thermotolerance acquisition during heat acclimation.[13] They activate HSP transcription and maintain a high long-term HSR by activating other HSFs such as HSFA2 (a highly heat-induced HSF), HSFA3, and HSFA7a, which are considered HSP transcriptional regulators during heat stress recovery.[14] In addition, the whole system is inter-regulated by a positive feedback mechanism since although HSFA2 is self-induced, it also activates other HSFs, which in turn continue the feedback loops.[15−17] HSFs are also regulated by members of the mitogen-activated protein kinase network (MPK) as well as through sumoylation and second messengers such as H_2O_2, which modify their oxidation state,[18] localization, oligomerization, and activity.[19−21] Therefore, ROS induce HSF oligomerization[22] and binding to HSEs (heat shock elements).[5]

In turn, HSP transcription is regulated by HSF activation complexes formed so that they can either stimulate HSPs (SlHSFA1-SlHSFB1 heterodimers)[23] or suppress them (SlHSFB1 only).[24] In particular, in mammalian systems, the HSF1 monomer is inactive and binds DNA as a homotrimer.[25]

HSF and HSP production is regulated by a complex sequestration feedback model that maintains the HSF and HSP levels through the buffering action of the HSP70/90 complex.[24] In unstressed plants, hypo-phosphorylated, class A1 HSF sequestration by HSP90/70 leads to their degradation through the DREB2A interacting UPS-E3 ligase system.[26]

Nonlethal temperature increase induces plasma membrane fluidity, to which the membrane-embedded cyclic nucleotide ion channels (CNGCs) respond,[27] and the PLCs are activated hydrolyzing PIP2 into IP3 and DAG. Both events trigger Ca2+ entry from the periplasm on the one hand and the ER on the other, into the cytoplasm. Ca2+ binding to the CNGC-bound calmodulins activates kinases (CDPKs and MAPKs), leading to HSFA phosphorylation.[28,29] In addition, during temperature rise, the increasing number of misfolded proteins in the cytoplasm competes with the HSFAs for the HSP90/70 complex, which is forced to release the HSFA1s[29] that remain safe from degradation due to DRIP1/2 inhibition and DREB2A accumulation. Also, due to ROS production following the new toxic environment, HSFA1 forms oligomers (trimers), which translocate to the nucleus and bind to the HSEs, activating transcription.

HSFs and HSPs are also hormonally regulated. PYR/PYL/RCAR receptor binding to ABA produced following stress results in PP2C inactivation. Activation by SnrK2 phosphorylation then leads to transcription factor binding to the target genes, such as DREB2A binding on the heat stress elements (HSEs), spreading in a positive feedback manner the HSR mechanism.

More interestingly, the function of HFAs is finely tuned by a PPIase chaperone system that guarantees cell survival through their vitality for proper protein folding, targeting, and function as well as PPIase activity. It was shown that high-molecular-weight chaperones known as FKBPs coordinate the HSR system.[11,30,31] FKBPs participate in the signaling and cell trafficking pathways during growth, developmental, and stress responses through their multidomain system[32,33] that altogether aims at fulfilling the chaperone mission of these proteins.

Two of them, ROF1 and ROF2, regulate the HSFA2 activity. Through their tetratricopeptide repeat (TPR) domains that both possess, they bind HSP90 and HSFA2, positively regulating HSFA2 transcriptional activity (ROF1 binding) or downregulating it (ROF2 binding).[11] In particular, ROF1 suppression was shown to decrease the HSP expression following recovery from the 37 °C treatment,[31] negatively affecting thermotolerance, whereas the absence of ROF2 led to a high expression of the small HSPs, having a positive effect on thermotolerance.[11] In addition, a simultaneous transient expression of both ROF1 and ROF2 was shown to repress transcription of small HSPs.[11] Interestingly, ROF1 interacts with NBR1 (next to BRCA1 gene 1) and HSP90 to mediate recovery from heat stress via a macroautophagy mechanism. NBR-mediated degradation of HSP90.1 and ROF1 attenuates HSFA2-regulated HSP gene expression and represses HS response.[34] Apart from their involvement in heat stress in *Arabidopsis thaliana*, they have been shown to interact with salinity stress, cell trafficking, and autophagy-related phosphoinositides PI3P and PI3,5P2,[33,32] determining the plant germination ability under salinity and osmotic stress. In addition, they show a dramatic accumulation in extremophile organisms such as *Artemia franciscana* under extreme environments.[35]

Using both single ($rof1^-$, $rof2^-$) and double ($rof1^-/2^-$) ROF-FKBP mutants, we show that although ROF1 and ROF2 proteins differentially but also synergistically regulate HSR, their simultaneous suppression enhances accumulation of most HSP classes and HSP-related proteins during heat acclimation.

https://doi.org/10.1021/acsomega.3c06773
ACS Omega 2024, 9, 2391−2408

Interestingly, double suppression of ROF1 and ROF2 enhances accumulation of partners of the proteasome system independent of temperature treatment, whereas it suppresses metabolic and developmental functions such as photosynthetic and cell plate formation elements. We suggest that this is possibly due to a mechanism or mechanisms that minimize energy-consuming developmental processes and sustain protein quality control in their absence, ensuring the continuation of proper plant performance.

2. EXPERIMENTAL PROCEDURES

2.1. *A. thaliana* Growth and Characterization of the Mutated Lines. *A. thaliana* ROF mutated lines have been previously described and characterized.[33] Seeds of the mutated lines were grown in a growth chamber (22 °C, 16*l*/8d), and new seeds were collected in order to ensure homogeneous and efficient growth for the ensuing experiments. Mutated plants were reconfirmed using gene-specific primers as well as Western blotting as previously described.[33]

2.2. *A. thaliana* Seedling Growth and Heat Acclimation Conditions. *A. thaliana* seeds (about 100) were disinfected in Eppendorf tubes using 70% ethanol for 2 min with mild shaking. Ethanol was replaced using 1 mL of 10% Na + hypochlorite for 30 s followed by 1.2 mL for 5 min and mild shaking. Seeds were washed thoroughly with five sequential replacements of 1.2 mL of sterile H_2O. They were finally resuspended in 500 mL of H_2O, transferred to Petri dishes containing 0.8% agar, 0.44% MS, pH 6.5 using NaOH, and allowed to stand at 4 °C overnight. Next day, they were transferred to 22 °C temperature, where they remained in a semivertical position for 3 days. For the heat acclimation experiment, Petri dishes each containing one of the following WT and mutated lines—WT (Columbia), *rof1*$^-$ (ROFB), *rof2*$^-$ and *rof1*$^-$/2$^-$ (N_dKO, double mutant)—were transferred to 37 °C for 4.5 h. For the C (control) experiment, WT and mutants remained at 22 °C. The experiments were performed on triplicated Petri dishes for each *A. thaliana* WT and mutant. Three separate experiments were performed.

2.3. Sample Preparation for Western Blotting and Mass Spectrometry. At the end of each experiment, random samples (seedlings) selected from each Petri dish were placed inside a single Eppendorf tube and extracted for 30 s in 200 μL of sample buffer (20 mM Tris-Cl pH 6.8, 2% SDS, 10% glycerol, 0.1 M DTT, 0.1% bromophenol blue) using a polytron adaptor. An average of 20 seedlings was used for each extraction (forming a solid compact volume of 50 μL). Extracts of each triplicate set were fused into one sample. Samples were vortexed, boiled at 100 °C for 5 min, and centrifuged at 17 000*g* for 10 min inside a fixed-angle centrifuge. The supernatants were collected, frozen at −80 °C, and used in the ensuing experiments. Protein concentration was determined by using the RC DC protein assay (Biorad). Therefore, the overall procedure resulted in three biological replicas. ROF1 and ROF2 accumulation in each sample, both under control and heat acclimation conditions, was confirmed by Western blotting following sample electrophoresis in 10% acrylamide/bis(acrylamide) solution (37.5:1) (Applichem). The ROF1 antibody was used for both ROF1 and ROF2 detection as previously described.[33]

2.4. LC-MS/MS. The protein extracts were processed with the FASP protocol using a 10 kDa cutoff filtering system (Sartorius, VN01H02). 60 μg of total protein was used for each treatment, which was loaded on the column using 8 M urea/0.1 M Tris pH 8.5 buffer. Following centrifugation at 14 000*g* for 40 min, columns were washed twice with the urea buffer for 20 min each. After sample cleanup, the proteins were alkylated with IAA and digested overnight at 37 °C on top of the filter with 1 μg trypsin/LysC mix (mass spec grade, Promega).

The resulting peptide products were analyzed by a nano-LC-MS/MS system of the LTQ Orbitrap XL mass spectrometer coupled to a nano-RSLC (Thermo Scientific). Each sample was analyzed using a 6 h long gradient in two technical replicas. Peptide concentration was determined through nanodrop measurement at 280 nm, and the injection volume was calculated accordingly. 2 μg of peptides was preconcentrated with a flow of 3 μL/min for 10 min using a C18 trap column (Acclaim PepMap100, 100 μm × 2 cm, Thermo Scientific) and then loaded onto a 50 cm long C18 column (75 μm ID, particle size 2 μm, 100 Å, Acclaim PepMap RSLC, Thermo Scientific). The binary pumps of the HPLC (RSLC nano, Thermo Scientific) consisted of Solution A (2% (v/v) ACN in 0.1% (v/v) formic acid) and Solution B (80% (v/v) ACN in 0.1% (v/v) formic acid). The peptides were separated using a linear gradient of 4% B up to 40% B in 340 min at a flow rate of 300 nL/min. The eluted peptides were ionized by a nanospray source and detected by an LTQ Orbitrap XL mass spectrometer (Thermo Fisher Scientific) operating in the data-dependent mode (DDA). Full-scan MS spectra were acquired in the Orbitrap (m/z 300−1600) in the profile mode with the resolution set to 60 000 at m/z 400 and automatic gain control target at 10^6 ions. The six most intense ions were sequentially isolated for collision-induced (CID) MS/MS fragmentation and detection in a linear ion trap. Dynamic exclusion was set to 1 min and activated for 90 s. Ions with single charge states were excluded. Lock-mass of m/z 445,120025 was used for continuous internal calibration. Xcalibur (Thermo Scientific) was used to control the system and acquire the raw files.

The raw files were analyzed with MaxQuant (1.5.3.30) using the Uniprot database of *A. thaliana* and a common contaminant database using the Andromeda search. The error detection FDR was set at 1% for both proteins and peptides with a minimum length of seven amino acids, which was determined after reversing the database. Protein abundance was then calculated based on a spectrum smoothing (LFQ intensity). LFQ was determined with a minimum measurement fraction of 2. Search parameters included a molecular weight ranging from 350 to 5000 Da, a precursor mass tolerance of 20 ppm, an MS/MS fragment tolerance of 0.5 Da, and a maximum of two missed cleavages by trypsin, and methionine oxidation, deamination of asparagine and glutamine, and protein N-terminal acetylation were set as variable modifications. Carbamidomethylation was set as a fixed cysteine modification. The match-between-run function was enabled.

The statistical analysis was performed using Perseus (version 1.6.2.1). The proteins that were detected as potential contaminants and in the reversed database as well as those that contained less than two peptides were rejected. Valid protein filtering was 70% in at least one group. Imputation was based on Gaussian distribution. The mass spectrometry proteomics data have been deposited to the ProteomeXchange Consortium via the PRIDE[36] partner repository with the dataset identifier PXD044216.

2.5. Statistical and Bioinformatics Analyses. Principal component analysis (PCA) was performed on all technical and biological replicas of the WT and mutated groups, following multiple-sample tests (FDR 0.05) and ANOVA, using the Benjamini−Hochberg cutoff method (FDR: 0.05). Component

https://doi.org/10.1021/acsomega.3c06773
ACS Omega 2024, 9, 2391−2408

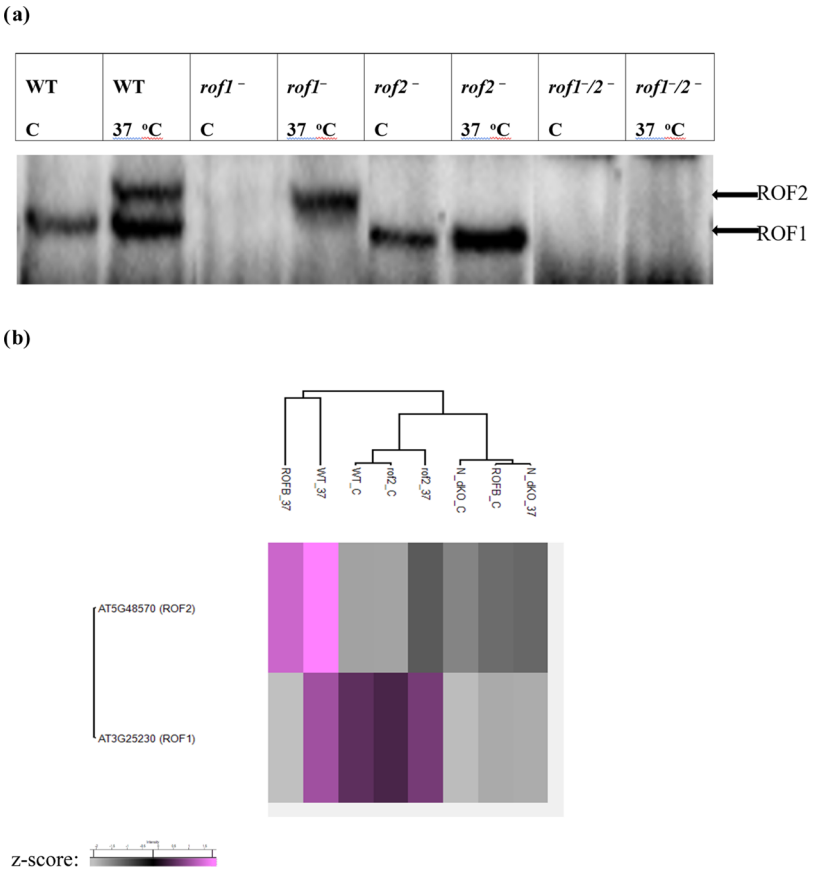

Figure 1. (a) Example of a heat acclimation experiment in *A. thaliana* WT and ROF mutated plants. Control (C): 22 and 37 °C heat-acclimated, for 4.5 h; seedlings were analyzed for ROF1 and ROF2 protein accumulation using anti-ROF1. WT and ROF1 mutated plants accumulated ROF2 following a 4.5 h heat acclimation, whereas ROF2 was not detected in *rof2*$^{-}$ and the double mutant *rof1*$^{-}$/*2*$^{-}$. Similarly, ROF1 accumulated independently of heat acclimation in both WT and ROF2 mutants and was not detected in *rof1*$^{-}$ (ROFB) and the double mutant. MW: ROF1:62 kDa; ROF2:65 kDa. (b) Heatmap (FDR: 0.05) following mass spectrometry for ROF1 and ROF2 accumulation in *A. thaliana* WT and ROF mutated plants.

1 and Component 2 are the first and second principal components in PCA, representing the directions in data space with the highest and second-highest variances, respectively. Volcano plots were performed between two samples following the *t* test (FDR: 0.05, S0:0.1). Significant values were selected, and the difference was calculated. Ontology analysis was performed using Metascape (https://metascape.org).[37] Enrichment analysis was performed using the following settings: minimum overlap 3, *P* value cutoff 0.01, and minimum enrichment 1.5. For meaningful comparisons, genes and Pathways/GO terms (provided from the Perseus analysis as well as Metascape) that were statistically over-/under-represented in the various comparisons were organized into tables with a custom Python script, where rows represented genes or Pathways/GO terms and columns represented different comparisons. Venn diagrams were constructed online (https://bioinformatics.psb.ugent.be/webtools/Venn/) and were used to identify common proteins for two or more mutations and/or conditions or unique for each condition and mutation. Intersections were calculated by entering a list of the Ensemble Gene identifiers produced following two-dimensional volcano comparisons of the ANOVA significance using Perseus analysis. The textual outputs produced by symmetric Venn diagrams indicating which elements are in each intersection or are unique to a certain list were used in our analysis.

For the multiple comparison of the protein accumulation profiles, the heatmap presentation was used. Significant values following the ANOVA test were selected (multiple-sample tests, FDR 0.05, number of randomizations 250). Replica values were averaged, and the means and median were calculated including SDs. Heatmaps were produced following *z*-scoring of the means and using the Euclidean distance. In order to determine which are the significant pairs of the ANOVA test, a post hoc analysis was performed on the significant findings of the ANOVA tests (FDR 0.05). Results of the post hoc tests, sequence coverage, and peptides for the ANOVA significant values are provided in Supporting data 1 (Table S1). Multiple comparisons between different samples of KEGG pathway enrichment were constructed in Perseus following multiple-sample tests and selecting the ANOVA significant values as described above. "KEGG pathway name" was selected as the unique category, and averaged (minimum size 3) and *z*-scoring of the means was performed before the multiple comparison.

3. RESULTS

3.1. Sample Characterization and Confirmation Prior to Mass Spectrometry Analysis. *A. thaliana* WT and mutated seedlings were confirmed for ROF1 and ROF2 protein accumulation prior to mass spectrometry analysis by Western blotting using anti-ROF1 as previously described.[33] Samples of all of the triplicate donor Petri dishes and from all three experiments were tested before being used in the mass spectrometry study (Figure 1a).

https://doi.org/10.1021/acsomega.3c06773
ACS Omega 2024, 9, 2391−2408

3.2. ROF1 and ROF2 Profiles in Mutated Control and Heat-Acclimated Plants. Sample nomenclature for the heat mapping and volcano plotting is described in Table 1.

Table 1. Sample Names Used in Mass Spectrometry and Presented in the Volcano Plotting and the Heat Mapping

	WT	*rof1*$^-$	*rof2*$^-$	*rof1*$^-$/2$^-$
C (control)	WT_C	ROFB_C	rof2_C	N_dKO_C
37 (37 °C)	WT_37	ROFB_37	rof2_37	N_dKO_37

Quantitative mass spectrometry confirmed the absence or the very low (below the significance threshold) abundance of ROF1 from both control and heat-stressed plants in the sample replicas of *rof1*$^-$. Similarly, it confirmed the absence of ROF2 from the heat-acclimated *rof2*$^-$ plants and the absence of both ROF1 and ROF2 from the *rof1*$^-$/2$^-$ double-mutated seedlings (Figure 1b). ROF2 was a highly accumulated protein in heat-stressed plants, and ROF2 protein levels accumulated in both the WT and *rof1*$^-$. ROF1 accumulated in both control and heat-stressed plants (Figure 1b), and an enhanced accumulation of ROF1 was detected under the 37 °C treatment in both the WT and *rof2*$^-$ plants. Also, see the "significant pairs" in the Supporting Information (Supporting data 1, Table S1).

3.3. Statistical Analysis. PCA was applied on all experimental samples used in LC-MS/MS analysis (three biological and two technical replicas) of the different groups, i.e., the WT and the mutated lines under control and heat-stressed conditions (Figure 2). When the control samples were compared to the heat-stressed ones (Figure 2a), the total cumulative contribution rates (TCCRs) of the first principal components (PCs) were 54.4 for the WT, 61.4 for the *rof1*$^-$, 52.8 for the *rof2*$^-$, and 52 for the *rof1*$^-$/2$^-$ double mutant, and a clear segregation could be observed between the control and the heat-stressed groups, showing a significant impact of heat stress on both the WT and the mutated lines. In addition, technical replicas were grouped together, confirming the reliability of the method and the data quality. Similarly, the different groups were compared (Figure 2b) under control (A) and heat acclimation (B), and a segregation pattern was observed between them, with the double mutant and the *rof1*$^-$ exhibiting the highest difference (TCCR: 60.1 for the control and 67.2 for the heat acclimation experiment).

3.4. KEGG Pathway, Ontology Analysis, and Profiles of Highly Enriched Proteins. KEGG pathway comparative analysis was performed by selecting the "KEGG pathway name" for the "averaged category" using Perseus 1.6.2.1. Comparatively highly enriched or suppressed categories for each group (the WT or the mutated lines) were plotted separately for the control and heat-stressed plants (Figure 3a,b).

The total number of KEGG pathways enriched in each group but suppressed in the others was also recorded (Table 2).

Ontology analysis was also performed using Metascape (Supporting data 1, Table S1), and specifically enriched pathway profiles were identified, and the top ones were selected and are summarized in Table 3. They show differential enrichment in protein folding, response to heat, ER processing, proteasome,

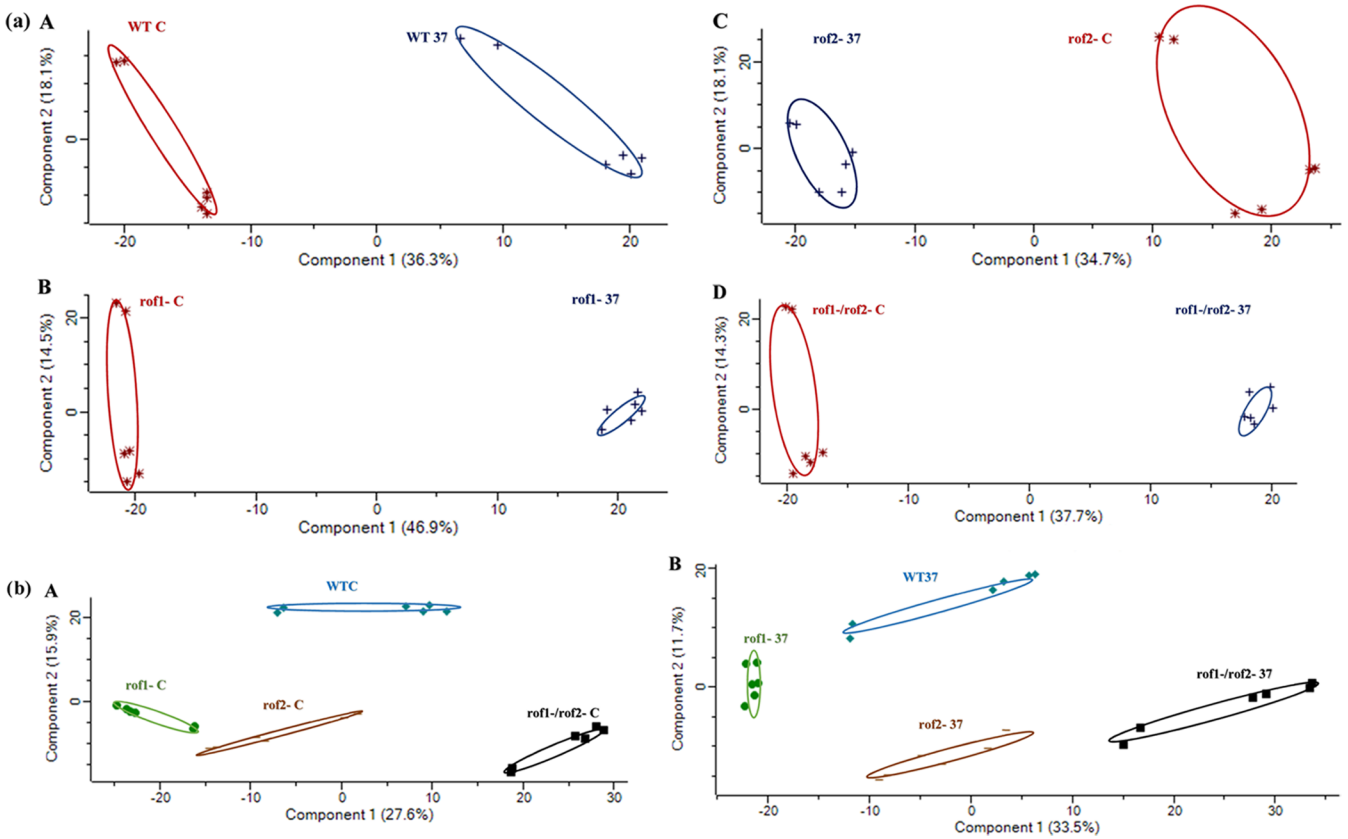

Figure 2. (a) Comparison of control (red stars) vs 37 °C heat-stressed plants (blue crosses) using PCA analysis of the WT (A) and the different mutated groups, *rof1*$^-$ (B), *rof2*$^-$ (C), and the double mutant (*rof1*$^-$/2$^-$) (D). (b) Comparison of the control (C) treatment between the different groups of mutated lines and the WT (A) and between the heat stress (37 °C) treatment of the different groups of the mutated lines and the WT (B).

https://doi.org/10.1021/acsomega.3c06773
ACS Omega 2024, 9, 2391−2408

(a)

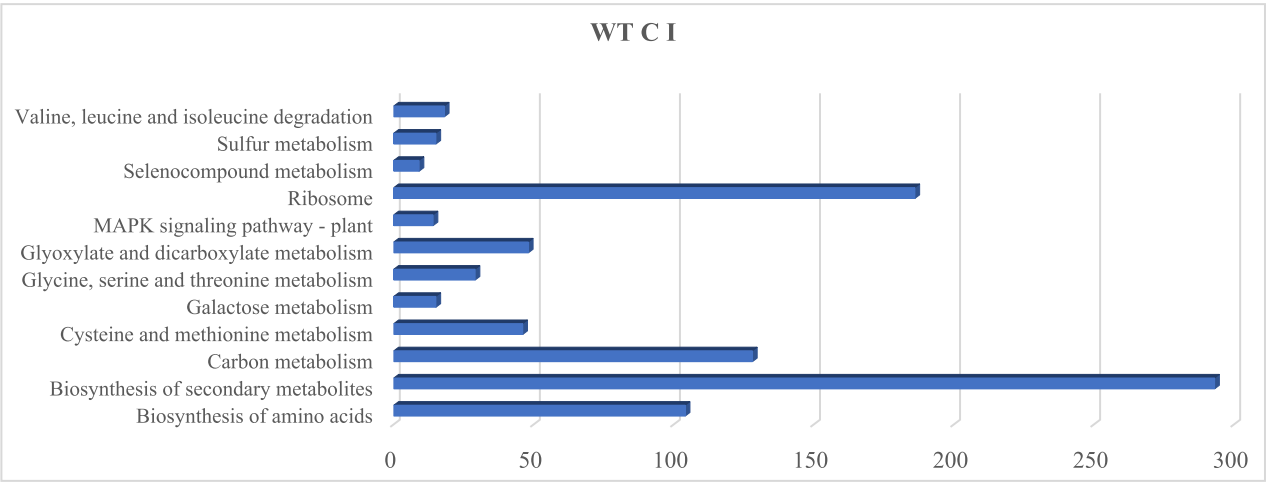

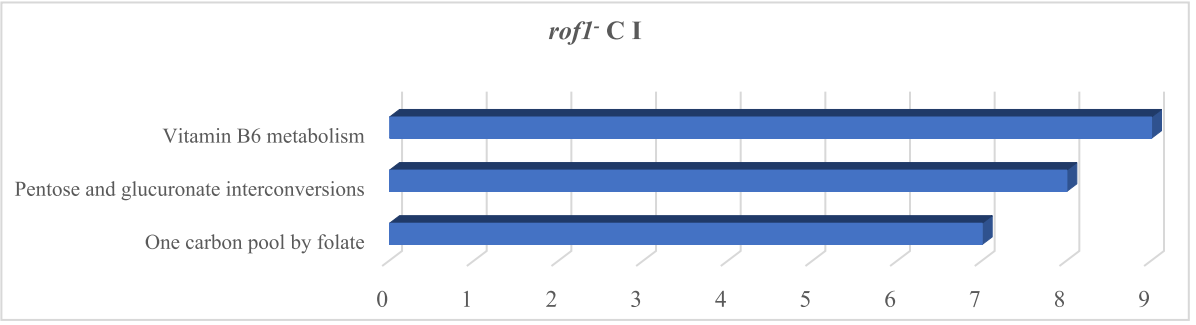

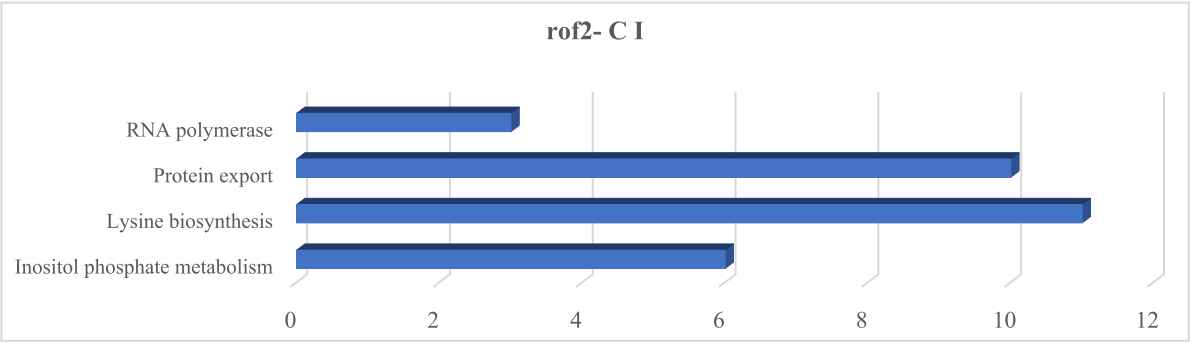

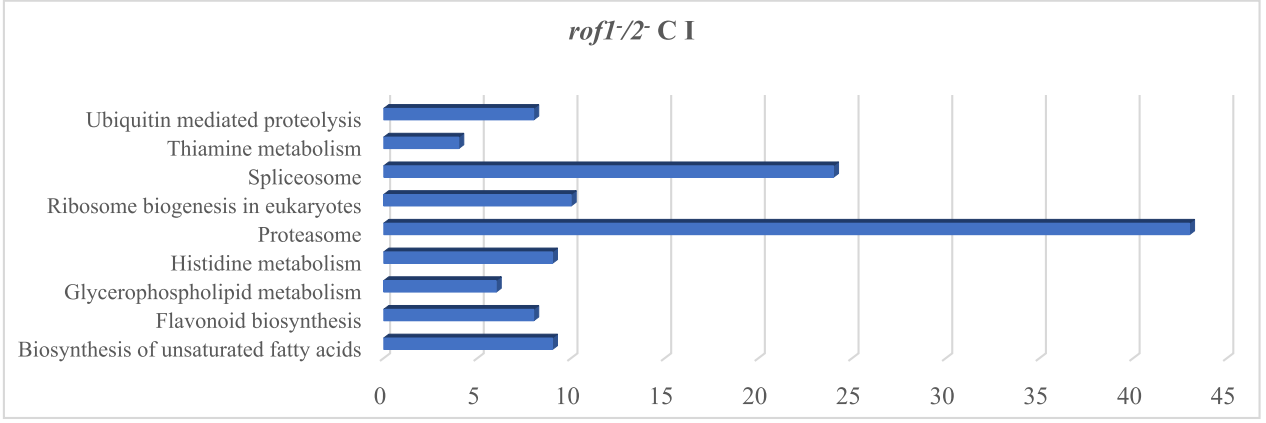

Figure 3. continued

https://doi.org/10.1021/acsomega.3c06773
ACS Omega 2024, 9, 2391−2408

(b)

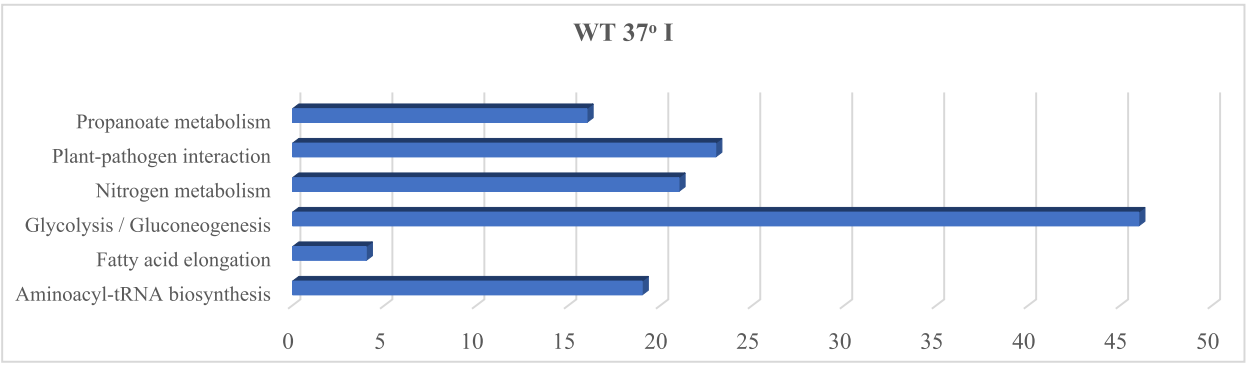

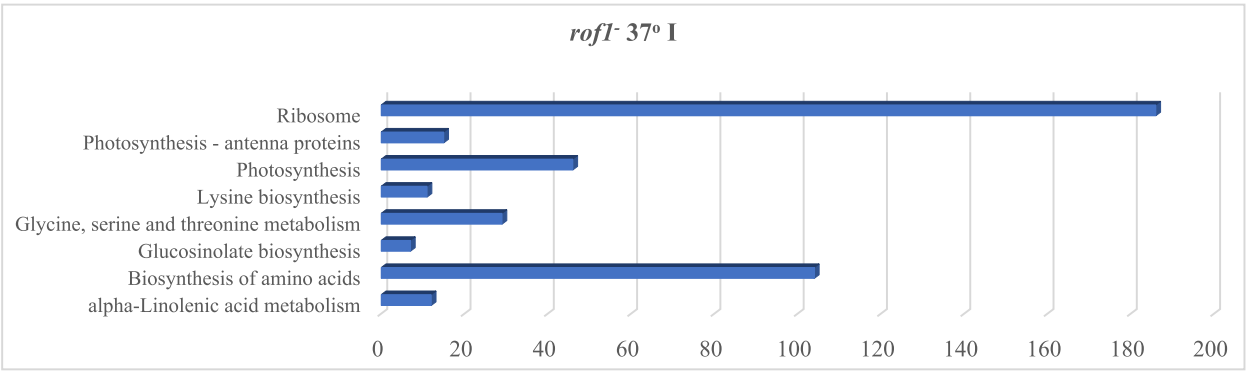

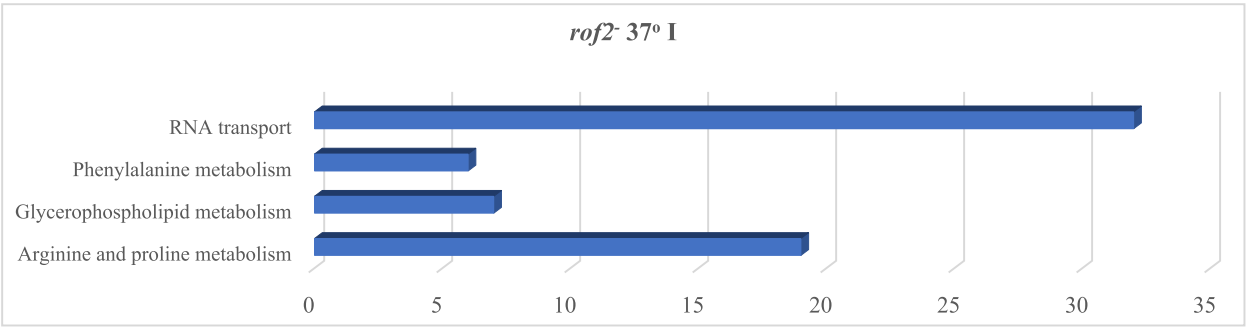

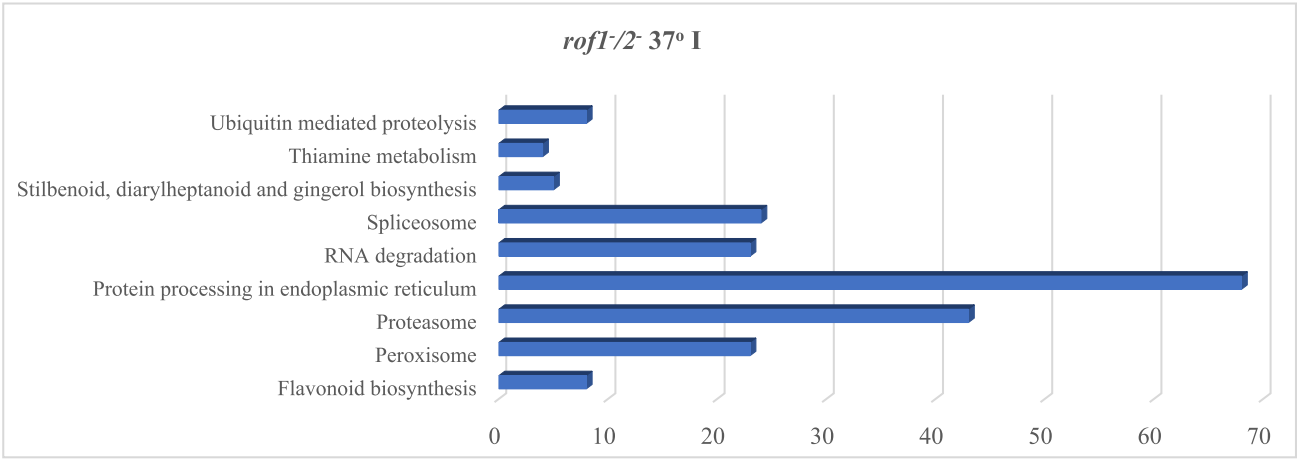

Figure 3. Comparative KEGG pathway enrichment under control (C, a) and acclimation heat stress (37 °C, b) between the WT and ROF mutants. The first highly enriched pathways of each group (WT or mutant) compared to all of the other groups under the control or heat stress conditions are shown. Y, pathway name; *X* axis, number of pathway members.

and the photosynthetic pathway as well as other biochemical and signaling pathways (Supporting data 1, Table S1).

Using Venn diagrams following a differential comparison of the proteomics data (Chart 1), 28 proteins were identified as

https://doi.org/10.1021/acsomega.3c06773
ACS Omega 2024, 9, 2391−2408

Table 2. KEGG Pathways Showing a Differential Enrichment between Different Groups under the Acclimation Condition[a]

	WT 37° S	*rof1*⁻ 37° S	*rof2*⁻ 37° S	*rof1*⁻/2⁻ 37° S
WT 37° I		5	12	18
rof1⁻ 37° I	9		7	42
rof2⁻ 37° I	8	5		4
rof1⁻/2⁻ 37° I	4	12	8	

[a]Numbers indicate the identical pathways enriched in one group but suppressed in another (I, enriched; S, suppressed).

bona fide heat-responding proteins accumulating in both the WT and ROF mutants at the completion of the 37 °C heat acclimation period (Table 4a). Furthermore, unique proteins for each treatment were identified to be preferentially suppressed or enriched in the WT and ROF mutants following the heat acclimation treatment (Table 4b).

3.5. Heat Stress Response. The heat response pathway in the WT and ROF mutants was studied using both summarized (KEGG pathway enrichment and Ontology analysis) and specific approaches focusing on proteins related to the HS mechanism. A high induction of the heat response pathway during heat acclimation compared to the untreated plants (control) independent of the mutation state was recorded (Table 3). Ontology analysis indicated that "protein folding", "response to heat", and the "protein processing in the ER pathway" show a similar pattern between mutants (Table 3). A thorough study of the participating proteins indicated that proteins of the "protein folding pathway" present in our samples

Chart 1. Venn Diagram of Accumulated Proteins Following the 37 °C Treatment in Both the WT and ROF Mutated Lines Compared to the Control Condition of Both the WT and the ROF Mutants[a]

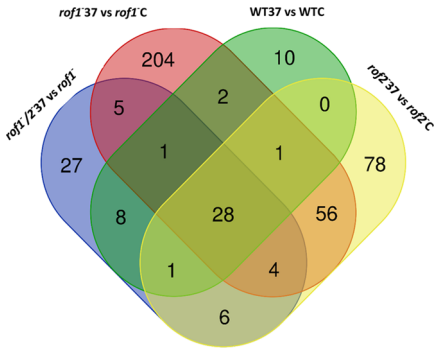

[a]28 proteins were identified to preferentially accumulate in all mutants and the WT (common proteins, Table 4a) following the 37 °C treatment compared to the control (22 °C) condition.

are also assigned to the "response to heat pathway" (53%). In addition, a high percentage of proteins belonging to the ER processing pathway is also assigned to the "protein folding" or "response to heat" or both pathways. However, even few proteins that belong to the ER processing pathway but not to the other two pathways (28%) showed a similar pattern to the ER processing and the other two pathways in total (not shown).

Table 3. Ontology Comparative Analysis of *A. thaliana* WT and ROF Mutated Plants (C: 22 and 37 °C Heat-Acclimated)[a]

description	protein folding	response to heat	protein processing in the endoplasmic reticulum	proteasome	ubiquitin-dependent protein catabolic process	photosynthesis
rof1⁻/2⁻ 37° vs *rof1*⁻/2⁻ C	−12.6248418	−25.70733	−24.13763405	0	0	0.437447071
rof1⁻/2⁻ 37° vs rof2⁻ 37°	−9.48098772	−13.64459	−14.01994717	−11.130717	−2.677910251	4.661378605
rof1⁻/2⁻ 37° vs rof2⁻ C	−16.0714264	−21.09708	−15.56931792	−11.8768276	−3.082396519	5.659554713
rof1⁻/2⁻ 37° vs rof1⁻ 37°	−22.627401	−20.06139	−19.89487104	−18.5788919	−7.352884579	10.02942714
rof1⁻/2⁻ 37° vs rof1⁻ C	−18.0436331	−21.88376	−21.88376266	−8.16633333	−3.013017949	7.155080021
rof1⁻/2⁻ 37° vs WT 37°	−11.0345409	−8.373203	−10.04092877	−1.72134923	0	3.072656975
rof1⁻/2⁻ 37° vs WT C	−23.7015077	−21.59673	−24.09477047	−7.40744215	−2.104623078	12.10147406
rof1⁻/2⁻ C vs *rof2*⁻ 37°	3.620065612	11.585455	9.619490403	−17.845223	−4.963777728	5.35326456
rof1⁻/2⁻ C vs *rof2*⁻ C	0	0	0	−13.8144775	−3.707371252	4.7166439
rof1⁻/2⁻ C vs *rof1*⁻ 37°	2.511358175	5.2093953	2.924595404	−20.9600391	−5.032013584	13.6993395
rof1⁻/2⁻ C vs *rof1*⁻ C	−1.75691643	−1.0222	−2.311547131	−10.8779724	−3.528691583	8.061584393
rof1⁻/2⁻ C vs WT 37°	7.64020023	9.8579756	7.949480282	−16.8316315	−4.578927809	6.419505183
rof1⁻/2⁻ C vs WT C	−6.26080501	−3.113289	−3.870458537	−15.2233295	−4.889426623	11.36040762
rof2⁻ 37° vs *rof2*⁻ C	−4.44193817	−12.67606	−13.82337279	−0.40709836	0	0
rof2⁻ 37° vs *rof1*⁻ 37°	0	−1.340271	−2.541773558	0	0	3.395952779
rof2⁻ 37° vs *rof1*⁻ C	−4.26032929	−12.64916	−16.64271045	0	0	1.471938331
rof2⁻ 37° vs WT 37°	0	0.4237657	0	0	0	0
rof2⁻ 37° vs WT C	−7.9238222	−17.04996	−13.78502444	0	0	1.942131255
rof2⁻ C vs *rof1*⁻ 37°	3.468416633	5.8353343	3.242295232	0	0	4.354858898
rof2⁻ C vs *rof1*⁻ C	0	0	0	0	0	0.448406493
rof2⁻ C vs WT 37°	5.134267988	13.283696	8.045234511	0	0	0.161717591
rof2⁻ C vs WT C	0	0	0	1.50029536	0	2.355596587
rof1⁻ 37° vs *rof1*⁻ C	−7.52627186	−9.91815	−8.44216373	−2.08879569	0	−0.820494957
rof1⁻ 37° vs WT 37°	3.364008089	3.1394925	2.401818918	0	0	−1.299769212
rof1⁻ 37° vs WT C	−3.4810175	−9.492165	−9.692320397	0	0	−0.333415175
rof1⁻ C vs WT 37°	8.20810811	11.178782	10.61183338	0.66638995	0	−1.857063667
rof1⁻ C vs WT C	4.132365176	2.4203843	1.026401053	2.22848889	0.644574533	0.186627783
WT 37° vs WT C	−6.98199572	−23.57513	−22.71576764	0	0	0

[a]Negative values indicate enrichment of the pathway in the first component vs the second component, whereas positive values indicate suppression.

https://doi.org/10.1021/acsomega.3c06773
ACS Omega 2024, 9, 2391−2408

Table 4a. Proteins Identified as Accumulated (Chart 1) or Suppressed Following the 37 °C Treatment in the WT and ROF Mutated Lines Compared to Their Control Samples

gene name	ensemble gene
accumulated	
ALY3	AT1G66260
APX2	AT3G09640
At2g20560	AT2G20560
BAG6	AT2G46240
CLPB1	AT1G74310
CLPB3	AT5G15450
ERD10	AT1G20450
FeslA	AT3G09350
HSP17.4A	AT3G46230
HSP17.4B	AT1G54050
HSP17.6	AT5G12020
HSP17.6B	AT2G29500
HSP17.6C	AT1G53540
HSP17.7	AT5G12030
HSP17.8	AT1G07400
HSP18.1	AT5G59720
HSP22.0	AT4G10250
HSP23.6	AT4G25200
HSP25.3	AT4G27670
HSP26.5	AT1G52560
HSP70-5	AT1G16030
HSP70-8	AT2G32120
HSP90-1	AT5G52640
MBF1C	AT3G24500
MED37C	AT3G12580
RPL5B	AT5G39740
T22K18.16	AT3G10020
T22P22_70	AT5G11680
suppressed	
GRP7;RBG7	AT2G21660
STR2	AT1G16460

Following the ontology study, a detailed analysis of HS-related proteins was performed by first focusing on HSP accumulation. HSP accumulation at the end of the heat acclimation period was assessed by analyzing HSP classes separately. Therefore, HSPs were divided into five groups (HSP20s, 60s, 70s, 90s, and 100) and presented by heat mapping (Figure 4) and volcano plotting (Supporting data 2, Figure S1). Heat-stressed WT plants accumulated higher HSP levels compared to the heat-stressed single mutants of ROF1 (HSP17.7, HSP90-1, CLPB1, CLPB4, CCT2, HSP23.6, HSP23.5, HSP15.7, CLPB3, MED37C, HSP70-5, HSP26.5, and HSP17.4B) and ROF2 (HSP17.4B, HSP18.1, and HSP70-5). Loss of both ROF1 and ROF2 functions resulted in a higher accumulation of HSP proteins following a 37 °C treatment, compared to the WT (small HSPs: HSP17.4A, 17.6B, 17.6C, 21, 23.6, 26.5, HSP70s: HSP70-10, 70-15, 70-3, 70-5, 70-9, HSP90s: HSP81-2, 90-2, 90-1, 90-6, CPN60, CPN10, and CLPB3), to ROF1 (small HSPs: HSP15.7, 17.4A, 17.4B, 17.6, 17.6B, 17.6C, 17.7, 17.8, 21, 22.0, 23.5, 23.6, 26.5, HSP60: CCT2, CCT3, CCT4, CCT7, CPN60, CPN60B2, CPN60B3, HSP70: HSP70-10, Hsp70-15, HSP70-15, HSP70-3, HSP70-5, HSP70-8, HSP70-9, MED37A, MED37C, MED37E, MED37F, HSP90: HSP81-2, HSP90-2, HSP90-1, HSP90-3, HSP90-6, HSP100: CLPB1, CLPB3, CLPB4), and to ROF2 (small HSPs: HSP17.4A, HSP17.4B, HSP17.6, HSP17.6B, HSP17.6C, HSP17.7, HSP17.8, HSP18.1, HSP21, HSP22.0, HSP23.6, HSP26.5, HSP70: HSP70-3, HSP70-5, HSP70-7, HSP70-9, MED37C, MED37E, HSP90: HSP81-2, HSP90-1, HSP100: CLPB1, CLPB3, CLPB4) mutants. In addition, the absence of either ROF1 or ROF2 resulted in a differential accumulation of the heat stress-related proteins at 37 °C, with a volcano plot analysis indicating a higher accumulation of proteins of the heat response pathway in the *rof2*$^{-}$ plants compared to the *rof1*$^{-}$ plants (HSP21, HSP23.5, HSP26.5, HSP81-2, HSP90-1, HSP90-3) (Figure 4 and Supporting data 2, Figure S1).

HSF factors were not detectable in the samples due to the low levels required for their function; however, proteins regulated by them showed a differential accumulation between mutants at the end of the acclimation period. In particular, proteins wherein the mRNA levels have been reported to be regulated by HSFA2[1] showed a higher accumulation in the double mutant compared to the single *rof1*$^{-}$ and *rof2*$^{-}$ where HSFA2-related proteins were, in some cases, also suppressed compared to the WT (Figure 5a). The low-temperature-induced (LTI65) protein

Table 4b. Proteins that Show Preferential Accumulation or Suppression in ROF Mutants at 37 °C Compared to the WT and the Other ROF Mutants under Control and Acclimation Treatment (I, accumulation; S, suppression)

rof1^{-}/*rof2*$^{-}$ (I)	ensemble gene	*rof1*$^{-}$/*rof2*$^{-}$ (S)	ensemble gene	*rof1*$^{-}$ (I)	ensemble gene	*rof1*$^{-}$ (S)	ensemble gene	*rof2*$^{-}$ (I)	ensemble gene
CDC48D	AT3G53230		AT1G29670	MBG8.21	AT5G54940		AT5G16400	ycf4	ATCG00520
CLPB3	AT5G15450	XTH4	AT2G06850		AT5G03900	CATHB3	AT4G01610	ASP1	AT2G30970
HSP17.4A	AT3G46230	PGM1	AT1G09780	ECI2	AT4G14430		AT4G36700		AT5G19100
HSP17.6B	AT2G29500		AT3G20820	SDR1	AT3G61220	CRD	AT1G03890	FDH1	AT5G14780
HSP17.6C	AT1G53540	MAP1B	AT1G13270	DHDPS1	AT2G45440	RGGB	AT4G17520	KAS2	AT1G74960
HSP23.6	AT4G25200	CHLI1	AT4G18480	FLA9	AT1G03870			PORB	AT4G27440
HSP26.5	AT1G52560	CHLD	AT1G08520	psbH	ATCG00710			5-METHYLT HIORIBOSE	AT2G05830
HSP70-3	AT3G09440			XTH24	AT4G30270				
HSP81-2	AT5G56030			PAT1	AT5G17990				
HSP90-1	AT5G52640			CBBY	AT3G48420				
LEA7	AT1G52690			BGLU34	AT1G47600				
MBF1C	AT3G24500			cox2	ATMG00160				
PAP1	AT4G04020								
PDX12	AT3G16050								
	AT5G53140								

https://doi.org/10.1021/acsomega.3c06773
ACS Omega 2024, 9, 2391−2408

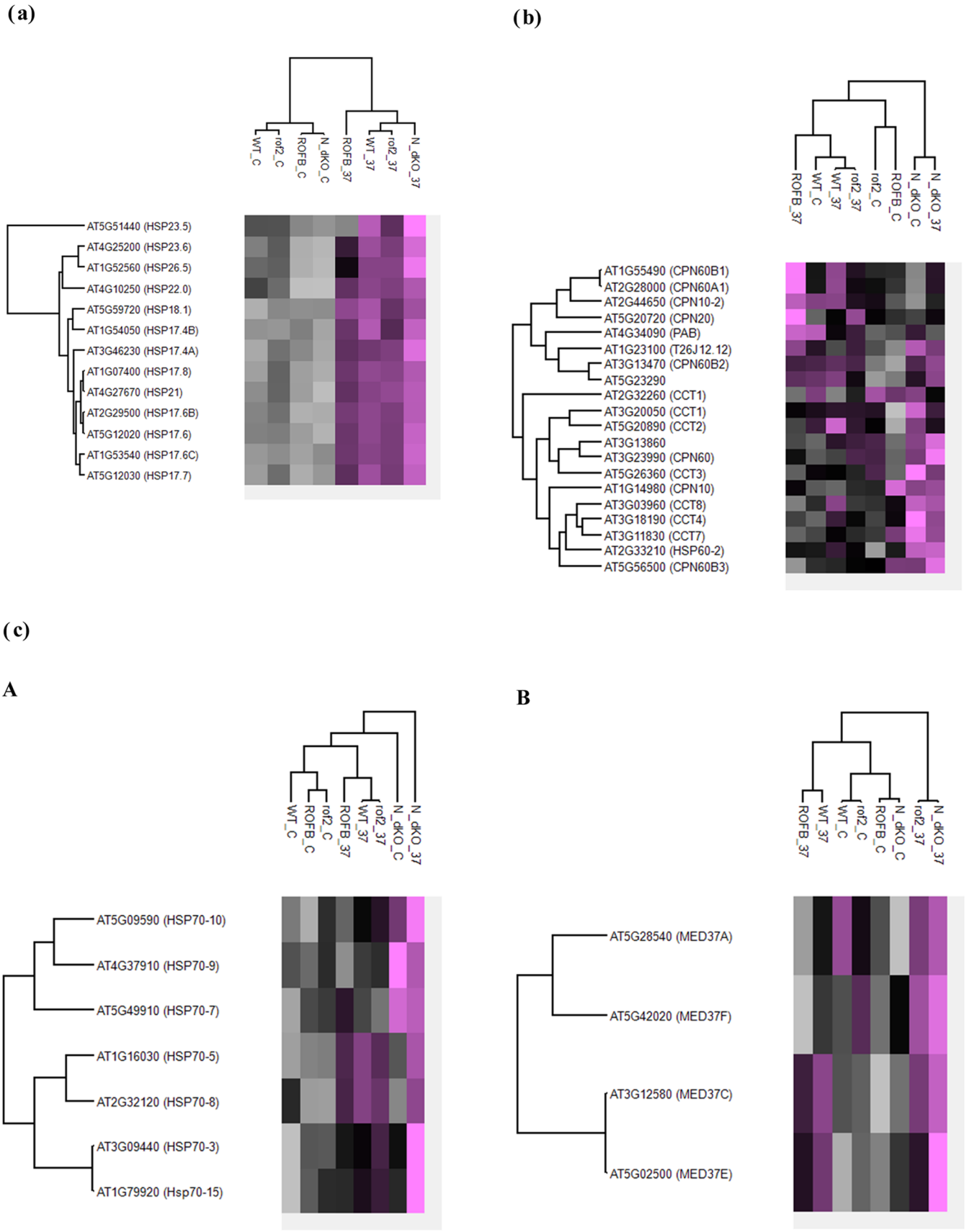

Figure 4. continued

https://doi.org/10.1021/acsomega.3c06773
ACS Omega 2024, 9, 2391−2408

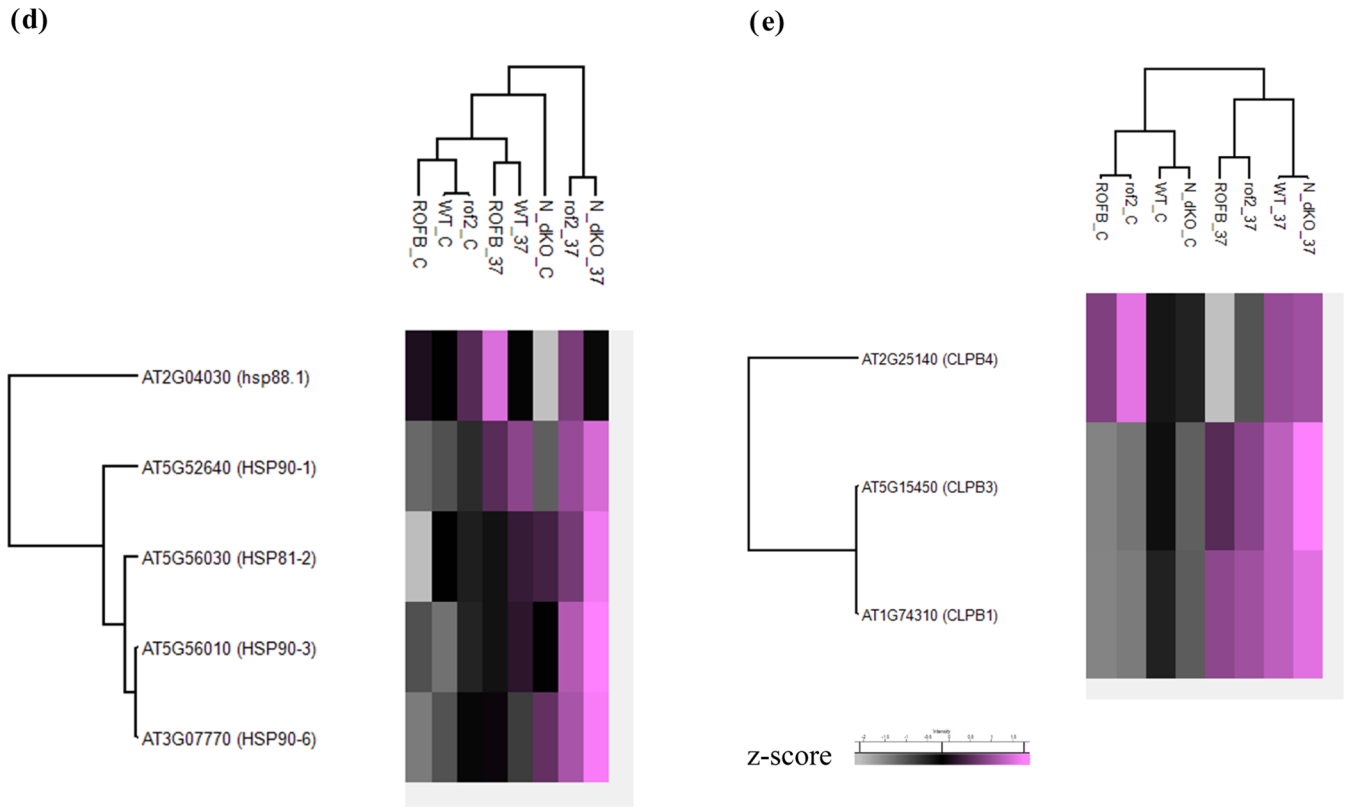

Figure 4. Differential accumulation of the HSPs in ROF mutants and the WT: (a) HSP20, (b) HSP60, (c(A)) HSP70, (c(B)) MED, (d) HSP90, (e) HSP100.

accumulated following the acclimation treatment only when both ROF1 and ROF2 were absent in both untreated and acclimated seedlings. On the other hand, the HSFA2-regulated peroxidase 27 was suppressed by the ROF mutations. Similarly, proteins belonging to the HSF1 "reactome" were identified using Perseus 1.6.2.1 and shown using volcano plotting. They also follow an enhanced accumulation pattern in the double mutant with the exemption of HSBP, GRF8, and GRF9, which were suppressed (Figure 5b). A differential accumulation in the double ROF mutant was observed for the HSP90/HSP70 organizing proteins (HOPs) that mediate binding of the client proteins to HSP90 (Figure 5cA). In particular, HOP1 appeared suppressed in all ROF mutations compared to the WT following the 37 °C treatment; however, this suppression was below the 0.05 threshold level. Its homologue HOP3 showed a similar accumulation pattern to the HOP1 interacting protein HSP70 (MED37C) (Figure 5cB), and both accumulated following the 37 °C treatment. Finally, the HSP70 cochaperones (NEFs) including FES1A, BAG6, and BAG7 were found differentially regulated between WT and the mutated lines (Figure 5d), with their interacting ubiquitin-related component RAD23 suppressed in the double mutation following acclimation.

3.6. Autophagy, Proteasome, and Ubiquitin-Dependent Protein Catabolism. The double mutation of ROF1 and ROF2 resulted in accumulation of the autophagy components CDC48D and CDC48A. In particular, the double mutation enhanced the CDC48A compared to all of the other conditions (Figure 6). Furthermore, the double mutation enhanced the accumulation of other proteins critical for the Cdc48-dependent protein degradation through the proteasomal degradation pathway, Ufd1 and Dsk2 (Figure 6).

Components of the proteasomal pathway preferentially accumulated in *rof1*$^{-}$/*2* $^{-}$ seedlings under both the control and the 37 °C treatment (Figures 3 and 7, Table 37). This pattern was reversed for certain mainly ubiquitin-related proteins involving the RAD23 ubiquitin receptor where the single ROF mutants showed enrichment at 37 °C compared to the double mutant (Figure 5dA and Supporting data 1, Table S1). A thorough study suggests suppression of certain proteasomal components under acclimation temperature compared to the control in the double mutant (Figure 7 and "significant pairs" in Supporting data 1, Table S1). A temperature effect on the proteasome-related components was also detected when comparing the *rof1*$^{-}$ at 37 °C to the *rof1*$^{-}$ C as well as the *rof2*$^{-}$ at 37 °C to the *rof2*$^{-}$ C (Table 3).

3.7. Photosynthesis. Our data suggest that all ROF mutations significantly affect genes involved in the photosynthetic processes. Specifically, both *rof1*$^{-}$ and *rof2*$^{-}$ showed enhanced accumulation of the photosynthesis-involved proteins compared to the double mutant (Table 3, Figure 8). The *rof1*$^{-}$ showed enhanced enrichment in photosynthetic partners even when compared to the WT at 37 °C. Temperature appeared to have an enhancing effect on certain members of the photosynthetic activity in the *rof1*$^{-}$ and a suppressing effect in some members in the double mutant at the end of the acclimation period (Table 3, Figure 8).

3.8. Cell Division. The single mutation, *rof1*$^{-}$, enhanced cell plate protein enrichment for the dynamine-related proteins (DRPs) compared to the *rof1*$^{-}$/*2*$^{-}$ under control conditions. In the double mutation, the other identified components of the cell plate were repressed compared with all of the other mutations and treatments. This effect was temperature-independent. In particular, the sec14 homologues, patellins 1, 2, and 4, were

https://doi.org/10.1021/acsomega.3c06773
ACS Omega 2024, 9, 2391−2408

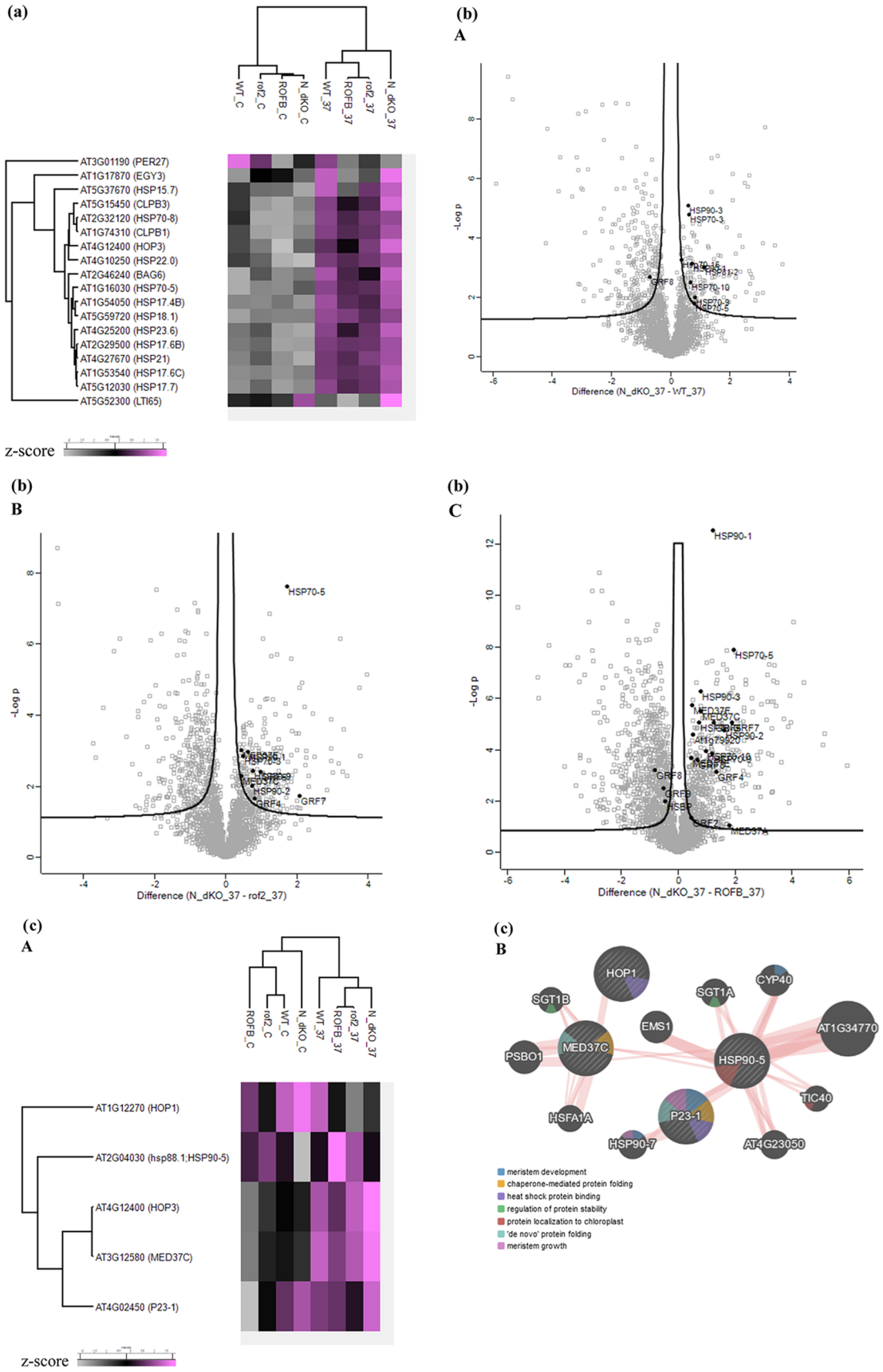

Figure 5. continued

https://doi.org/10.1021/acsomega.3c06773
ACS Omega 2024, 9, 2391−2408

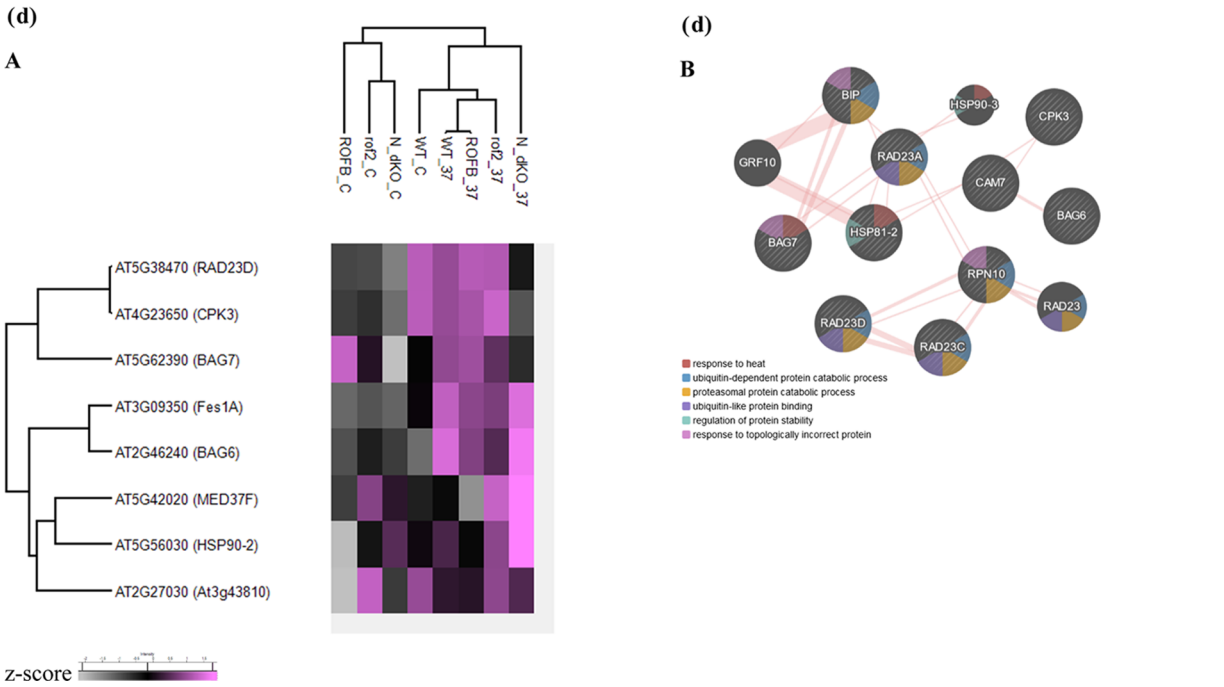

Figure 5. Differential accumulation of HSR proteins and their interactome. (a) HSFA2-regulated proteins and (b) accumulation of proteins of the HSF1 interactome (A) Hsp70-15, HSP70-15, HSP70-3, HSP90-1, HSP90-3, HSP90-2, HSP70-9, HSP70-10, and HSP70-5 are enriched in *rof1*$^{-}$/2^{-} compared to the WT, while the GRF8 is suppressed; (B) HSP70-3, HSC70-1, MED37E, HSP90-1, GRF5, GF14, GRF4, HSP90-2, HSP70-9, GRF7, MED37C, and HSP70-5 are enriched in *rof1*$^{-}$/2^{-} compared to the *rof2*$^{-}$; and (C) Hsp70-15, HSP70-15, HSP70-3, HSC70-1, MED37E, HSP90-1, GRF3, GRF5, GF14, GRF4, HSP90-3, HSP81-2, HSP90-2, BIP2, MED37F, HSP70-9, GRF7, HSP70-10, MED37C, MED37A, and HSP70-5 are enriched in *rof1*$^{-}$/2^{-} compared to the *rof2*$^{-}$, while the GRF8, GRF9, and HSBP are suppressed. (c) Accumulation patterns of the HOP interactome members. (d) Accumulation patterns (A) of the members of the NEF network (B).

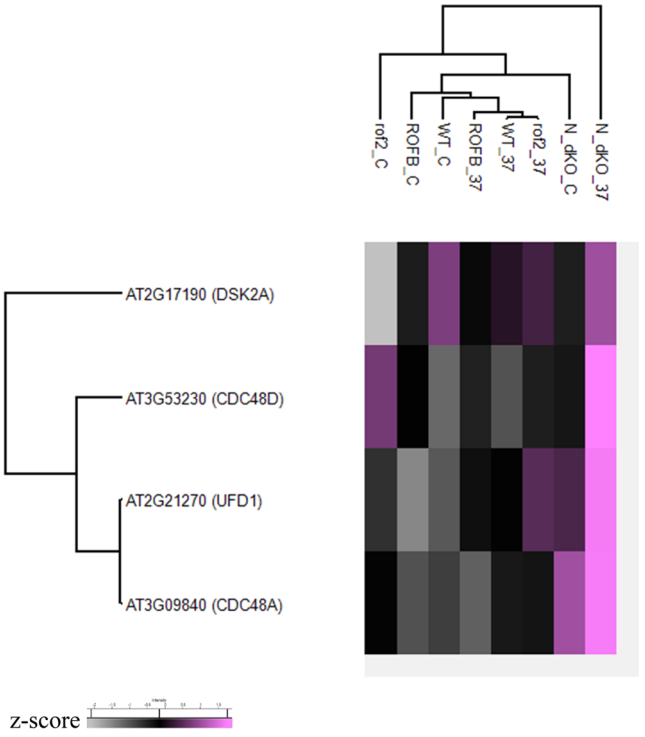

Figure 6. Differential accumulation of the components of the UFD pathway.

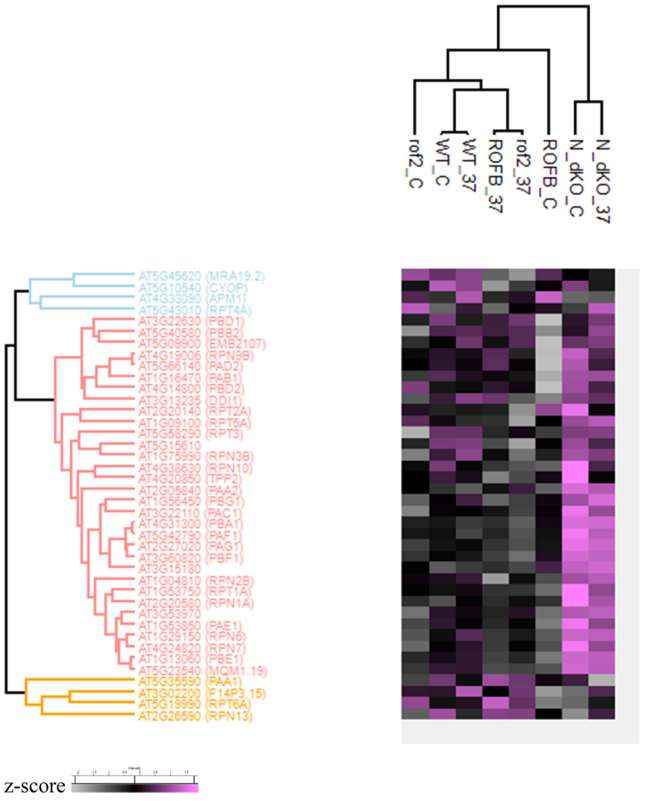

Figure 7. Differential accumulation of the proteasome/ubiquitin system.

enriched in the WT and the single mutants both in the control and at the end of the acclimation period, but this enrichment was abolished in the double mutation (Figure 9). Other differences

https://doi.org/10.1021/acsomega.3c06773
ACS Omega 2024, 9, 2391−2408

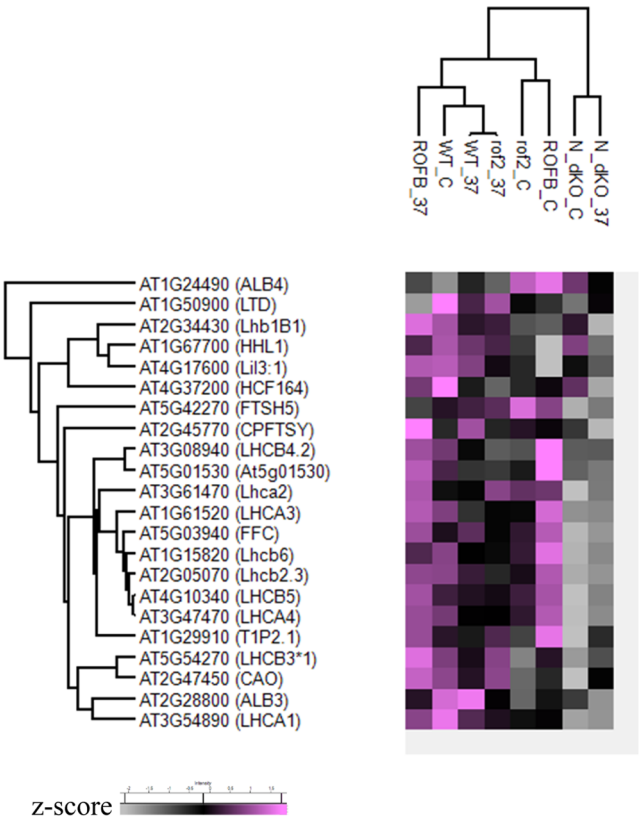

Figure 8. Differential accumulation of the photosynthetic components of the light-harvesting complex (LHC).

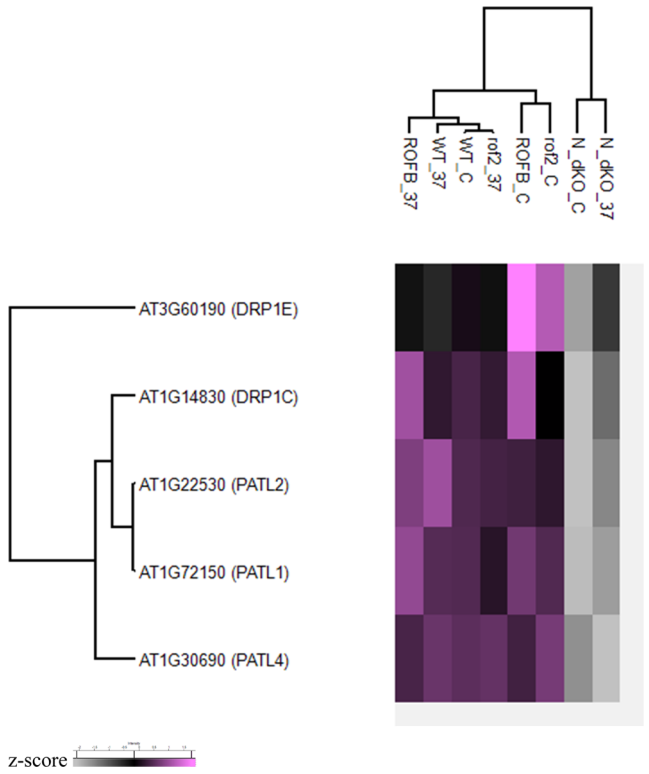

Figure 9. Differential accumulation of the cell plate components involving three patellin (PATL) isoforms and two dynamin-related proteins (DRPs).

observed between mutants and treatments were below the 0.05 threshold level.

4. DISCUSSION

A. thaliana WT and three mutated lines, the two single mutants of ROF1 (*rof1*$^-$) and ROF2 (*rof2*$^-$) and the double mutant *rof1*$^-$/*2*$^-$, were used in a differential screening mass spectrometry study in order to perform an in-depth evaluation of the role of these two key HS response regulators during HS acclimation, in plants.

ROF1 and ROF2 proteins accumulate at 37 °C (acclimation temperature) (Figure 1) and remain stable for at least 4 h upon recovery.[30] The same study showed that ROF2 expression is downregulated in hsfa1 mutants, suggesting that ROF2 expression might be regulated by the HSFA factor.

The developmental and HS response role of ROF1 and ROF2 homologues in plants was first described for their wheat orthologues FKBP73 and FKBP77.[38−40] It was shown that the two developmentally regulated FKBPs differentially accumulate during stress, with FKBP77 being the one responding and accumulating following HS. Both FKBPs were shown to bind HSP90 in a heterocomplex via their TPR domain. Transgenic plants overexpressing wFKBP77 accumulated higher levels of hsp90 transcripts. In *A. thaliana*, ROF1-HSP90 complexes assemble in vivo and their formation is regulated by environmental conditions such as heat stress and hormones.[30] In *A. thaliana*, HSFA2 interact with the HSP90-ROF1 complex, they localize in the nucleus, and they are responsible for keeping the levels of small HSPs during the recovery following the acclimation period.[11] Nuclear localization of ROF1 was shown to be HSP90- and HsfA2-dependent.[31] ROF2 does not interact with HSP90.1, and its involvement in the HSP90.1-HSFA2 complex was suggested via its ROF1 partner. ROF1−ROF2 complexes were detected in both nuclei and the cytoplasm, and ROF2 translocation to the nucleus occurred only during the recovery period and was HSP90.1/HSFA2-independent. In the *rof1*$^-$, the level of small HSPs was shown reduced following a 37 °C treatment and recovery for 24−48 h, and this correlated with a collapse of the *rof1*$^-$ plants following a 45 °C incubation after the acclimation and recovery period.[31] In contrast to the ROF1 effect, absence of ROF2 led to a high expression of small HSPs following the recovery period, and this was correlated with HS resistance of the *rof2*$^-$ plants.[11] Therefore, despite the high homology (85%) of the two genes, ROF1 and ROF2 proteins seemed to have an antagonistic role, which was correlated with their transgenic plant behavior (*rof1*$^-$ and *rof2*$^-$ and ROF1OE). However, there was no clear functional evidence regarding the plant response to heat stress in the absence of both *rof1*$^-$ and *rof2*$^-$ (*rof1*$^-$/*2*$^-$ double mutant). Transient expression of both ROF1 and ROF2 abrogated HSFA2 transcriptional activity, but a clear phenotype was not detected in the *rof1*$^-$/*2*$^-$ double mutant—a fact that was attributed to an antagonistic role of the two proteins.[11]

These studies followed the expression of a specific group of genes mainly at the transcriptional level. Regarding the acclimation period, Western blotting approaches may not have been sufficient to identify differences in detail among the WT, *rof1*$^-$, and *rof2*$^-$ regarding the sHSP accumulation.[11] In the present study, we follow a detailed two-dimensional LC-MS/MS protocol in order to identify and study events at the completion of the acclimation period using both single (*rof1*$^-$ and *rof2*$^-$) and double (*rof1*$^-$/*2*$^-$) mutants and compare them to each other as well as to the WT.

https://doi.org/10.1021/acsomega.3c06773
ACS Omega 2024, 9, 2391−2408

Following data uploading and study using the Perseus program, the PCA analysis showed segregated patterns between the different mutants and treatments and close grouping of the technical replicas, confirming the reliability of the experiment (Figure 2). Our results show that ROF2 is a bona fide heat stress protein as previously shown.[11] Higher accumulation of ROF1 in the WT C compared to that in the *rof2*$^{-}$ C was far below the significance threshold level (FDR: 0.05 and 0.1). The same applies to ROF1 and ROF2 detection in their single (*rof1*$^{-}$ and *rof2*$^{-}$ respectively) and double mutants.

Ontology analysis and Venn diagrams, where the lists of significantly differentially accumulated proteins were introduced following Perseus data analysis, indicate variability in pathways and proteins enriched in different mutants and the WT (Tables 3 and 4a). The double ROF mutant shows an enriched proteome regarding the representation of the heat stress response, protein folding, ER processing, and the proteasome pathway. KEGG pathway analysis (Figure 3 and Table 2) suggests that the *rof1*$^{-}$/*2*$^{-}$ proteome shows an "opposite trend" mainly to the *rof1*$^{-}$ proteome and to a less extent to the *rof2*$^{-}$ proteome (Table 2). On the other hand, many components of photosynthesis such as the LHCs are abrogated in the double mutant (Table 3, Figure 8). In contrast to the double mutation, single ROF1 and ROF2 mutants do not shift the accumulation balance toward the HSPs. *rof1*$^{-}$ tends to preferentially accumulate proteins related to cell wall biosynthesis. Such proteins include FLA9 (fasciclin-like arabinogalactan protein 9) involved in secondary cell wall biogenesis and TH-24 (xyloglucan endotransglucosylase) involved in cell wall biogenesis, organization, and loosening as well as xyloglucan metabolic processes, suggesting an enhanced ability of germination in the *rof1*$^{-}$.

Following the heat acclimation treatment, HSP accumulation is suppressed in the single mutants compared to the WT 37 °C treatment. In contrast, the double ROF mutant accumulates significantly higher levels of the HSPs compared to those of the WT 37 °C treatment. This applies not only to the sHSPs but also to heat-induced large HSPs such as the HSP90-1 (Figure 4 and Supporting data 2, Figure S1).

HSFs were not identified in this study, and this is possibly due to their low abundance.[1] However, HSFA2 (known to interact with HSP90.1 in a ROF complex)-regulated proteins were identified to be preferentially accumulated in the *rof1*$^{-}$/*2*$^{-}$ but suppressed in the single mutant compared to the WT (Figure 5a). Similarly, proteins of the HSF interactome were also enriched in *rof1*$^{-}$/*2*$^{-}$ including most GRFs but not the HSBP, which was found specifically suppressed in both control and heat-stressed *rof1*$^{-}$/*2*$^{-}$ (Figure 5b).

The cytosolic HSP90s contain an MEEVD motif at their dimerizing site carboxy-terminal domain (CTD), which mediates the binding of tetratricopeptide repeat (TPR)-containing cochaperones. Similarly, HSP70s contain an EEVD motif at their C-terminus. Cochaperones as well as HSP90 client proteins bind in the middle HSP90 domain. The HSP90/HSP70 organizing protein (HOP) mediates binding of the client proteins to the HSP90 by interacting through its TPR motif with the C-terminal motifs of both HSP90 and HSP70.[41] Interestingly, it was demonstrated that ROF1 also binds HSP90.1 through its TPR domain in a manner that resembles HOP-HSP90 binding.[30] Two HOP homologues were identified by quantitative LC-MS/MS: HOP1 and HOP3. HOP3 followed a pattern identical to that of its interacting partner MED37C, and both were similar between WT and ROF mutants. The HOP3 protein accumulates following heat treatment, and this is in agreement with previous findings showing rapid accumulation of HOP3 transcripts following a 38 °C treatment for 3 h.[42] However, the redundant HOP1 homologue that has been shown to accumulate in control and heat stress[42] appears unaffected in the mutated ROF lines at 37 °C (Figure 5c and Supporting data 1, Table S1). Following the CTD-mediated dimerization and formation of the V-shaped HSP90 dimer, the amino-terminal domain (NTD)-containing nucleotide-binding domain (NBD) undergoes transient dimerization and NBD ATP binding, resulting in HSP90 activation.[43] The latter occurs by the dissociation of HSP40, HSP70, and HOP, which triggers ATP binding and binding of other cochaperones such as p23 (Figure 5cB), which leads to the formation of an ATPase-competent conformation[44] and was identified to be present in both the WT and ROF mutants following the 37 °C treatment. Therefore, the HOP-related mechanism does not appear to be significantly affected by the ROF mutations.

HSP70s are also composed of a highly conserved N-terminal nucleotide-binding domain (NBD) with ATPase activity and a substrate-binding domain (SBD). The ATP hydrolysis-generated energy is responsible for substrate processing. Therefore, HSP70s release their substrates following ADP liberation. HSP70s promote protein folding or refolding with the aid of the nucleotide exchange factors (NEFs),[45] which accelerate ADP disassociation. The Fes1A protein is a NEF that increases molecular chaperone efficiency, and its knockout results in HSP70 degradation and reduced thermotolerance. Bcl-2-associated-athanogene (BAG) proteins are also believed to function as NEFs. Competition between BAG1 and the Fes1 homologue HSPBP1 determines the carboxyl-terminus HSP70-interacting protein (CHIP)-dependent degradation of the HSP70 targeted protein. HSPBP1 prevents degradation by inhibiting the CHIP ubiquitin ligase activity (Fu et al. 2019).[46] The nuclear localized calmodulin binding protein BAG6 is highly expressed in response to HS and is an HSP70-binding protein that suppresses the expression of Fes1A via a calmodulin-related pathway and plays a positive role in thermotolerance in *Arabidopsis*.[46] In our mass spectrometry analysis, we identified two calmodulin binding BAG homologues: BAG6 and BAG7. A strong expression of BAG6 and Fes1A following heat stress in both WT and mutated plants can be observed. At the same time, the calmodulin binding CPK3 appears abrogated in the double mutant under heat stress compared to the WT (Figure 5d). BAG7 (a BIP binding protein) accumulation is abrogated in the control double mutant compared to that of the single ROF1. Its interacting partner, the ubiquitin receptor RAD23D, is abrogated compared to all other mutants and the WT under the acclimation temperature (Figure 5d). In contrast, BAG6 and Fes1A were identified to accumulate in heat-stressed plants independent of the mutation (Table 4a). The calmodulin binding protein BAG6 interacts with CaM3, which acts as a transcriptional activator of HSP18.2 and HSP25.3 (HSP20.1) under heat stress.[47] CaM3 (At2g27030) accumulation appears abrogated in the ROF1 control mutants, but its accumulation is not affected by heat stress compared to the other mutants and the WT (Figure 5d). Future work will elucidate the function of these HSR components and their relation to the heat acclimation factors.

Furthermore, the proteasome and autophagy-related proteins CDCD48A and CDC48D together with the autophagy-involved BAG6 accumulate in the ROF double mutant (Tables 4a and 4b, Figures 5dA and 6). CDC48, a central factor in proteasomal

https://doi.org/10.1021/acsomega.3c06773
ACS Omega 2024, 9, 2391−2408

degradation, was also identified to control lysosomal protein degradation, and its absence causes severe protein aggregation.[48] Both CDC48 and other important members of the ubiquitin fusion degradation (UFD) pathway, including Ufd1 and Dsk2, were enriched in the ROF double mutation (Figure 6). It has been demonstrated that heat stress memory is regulated in *A. thaliana* by the autophagic degradation of ROF1 and its interacting partner HSP90.1 during recovery from heat stress.[34] This degradation mediated by NBR1 results in an attenuation of the heat stress memory, HSFA inactivation, and HSP reduction. CDC48 is associated with NBR1 via RAD23 homologues. Only one RAD23 homologue was identified in our study as significantly suppressed in the double ROF mutant. RAD23 is an adaptor protein that binds to both ubiquitinated substrates and the proteasome and escapes degradation because it lacks an effective initiation region at which the proteasome can engage the protein and unfold it.[49] It is possible that in the absence of both ROF1 and ROF2, the HSP balance (production and degradation) is regulated by the presence or absence of specific components of the protein degradation mechanism such as RAD23. Although it has been suggested that RAD23 facilitates time-dependent coupling of signaling events to transcriptionally affected genes, it is possible that other such receptors may also play such fundamental roles.[50,51] It may be clearly observed that the double ROF mutant under both control and acclimation shows an enrichment in several components of the proteasomal pathway compared with the other mutants and the WT (Figure 7). This effect on some proteasomal components seems independent of the heat stress since their accumulation is enhanced in the double mutant when compared to the WT even under control conditions. This could be explained by the need for protein degradation in the double ROF mutant where enrichment in certain HSPs was observed compared to the WT and the other mutants even in the control (22 °C), a fact that may impede proper plant performance under nonthreatening conditions.

Implication of ROF1 and ROF2 in cell division is clearly identified by the effect of the double mutation on the accumulation of the patellin (PATL) homologues (Figure 9 and Supporting Information, Table S1). Patellins (PATLs) are sec14 homologues transferring lipids to the cell plate formed during cell division. Sec14 has been identified in a previous study to bind on PI3P and PI3,5P2 together with ROF1 and ROF2 following the use of PIP affinity chromatography.[32] All patellin isoforms are specifically suppressed in the ROF double mutant, implying a direct effect of the ROFs on cell division. A possible effect of ROF mutations on cell plate formation is further supported by an enhanced accumulation of the two identified dynamin-related proteins (DRPs) in the ROF1 mutant, an effect that is, however, abolished following heat treatment. Dynamin is involved in vesicle formation and membrane remodeling during cytokinesis and localizes to the expanding cell plate similarly to the PATLs.[52] The results suggest an opposite trend in the double mutation regarding cell plate formation, especially toward the single *rof1*$^{-}$ mutation. This is an interesting result since the ROF double mutants do not present any apparent developmental defect although a delayed growth was observed during the early stages of seedling development (results not shown). It is possible that other proteins may complement patellin and dsynamin functions or/and the double mutant may have ultrastructural nonlethal defects.

Conclusively, ROF1 and ROF2 are multifunctional proteins that not only coordinate stress responses through various mechanisms and protein quality control pathways but are also involved in developmental processes. This may be supported by the fact that the absence of both ROF homologues affects developmental and biochemical pathways not only in response to stress but even under nonstress conditions. Through their multifunctional role, they may synchronize protein quality control at all levels of plant growth, development, and environmental adaptation. During heat stress, both our present work and previous studies[11,30] have highlighted their collaboration in the development of heat stress acclimation; however, a previously suggested differential and possibly antagonistic role at certain levels of heat stress is also highlighted in the present study by the enhancement of heat acclimation-related components and protein quality control pathways in the absence of both proteins. Future functional studies of the identified differentially regulated proteins will elucidate their role in the ROF-regulated plant development of heat stress resistance.

■ ASSOCIATED CONTENT

Supporting Information

The Supporting Information is available free of charge at https://pubs.acs.org/doi/10.1021/acsomega.3c06773.

Mass spectrometry proteomics data have been deposited to the Proteome X change Consortium via the PRIDE partner repository with the data-set identifier PXD044216; results of the post hoc tests, sequence coverage, and peptides for the ANOVA significant values (Table S1); and Metascape ontology analysis (Table S2) (XLSX)

Volcano plotting of the preferential accumulation of the HSPs between mutants and the WT in 37 °C acclimated seedlings (Figure S1) (PDF)

■ AUTHOR INFORMATION

Corresponding Author

Theodora Farmaki − *Institute of Applied Biosciences, Center for Research and Technology—Hellas, 57001 Thermi Thessaloniki, Greece;* orcid.org/0000-0002-0293-5091; Phone: + 30 2310 498279; Email: mfarmaki@certh.gr

Authors

Paraskevi Lefa − *Institute of Applied Biosciences, Center for Research and Technology—Hellas, 57001 Thermi Thessaloniki, Greece*

Martina Samiotaki − *Biomedical Sciences Research Center "Alexander Fleming", Institute for Bioinnovation, 16672 Vari, Greece*

Complete contact information is available at: https://pubs.acs.org/10.1021/acsomega.3c06773

Funding

The work was supported by the "Development Grants for Research Institutions—KRIPIS" action.

Notes

The authors declare no competing financial interest.

■ ACKNOWLEDGMENTS

The authors would like to thank G. Amoutzias and M. Nikolaidis for help with the presentation of the Metascape results.

REFERENCES

(1) Echevarría-Zomeño, S.; Fernández-Calvino, L.; Castro-Sanz, A. B.; López, J. A.; Vázquez, J.; Castellano, M. M. Dissecting the proteome dynamics of the early heat stress response leading to plant survival or death in Arabidopsis. *Plant, Cell Environ.* **2016**, *39* (6), 1264−1278.

(2) Wang, W.; Vinocur, B.; Shoseyov, O.; Altman, A. Role of plant heat-shock proteins and molecular chaperones in the abiotic stress response. *Trends Plant Sci.* **2004**, *9* (5), 244−252.

(3) Mittler, R.; Finka, A.; Goloubinoff, P. How do plants feel the heat? *Trends Biochem. Sci.* **2012**, *37* (3), 118−125.

(4) Jarratt-Barnham, E.; Wang, L.; Ning, Y.; Davies, J. M. The Complex Story of Plant Cyclic Nucleotide-Gated Channels. *Int. J. Mol. Sci.* **2021**, *22* (2), 874.

(5) Volkov, R. A.; Panchuk, I. I.; Mullineaux, P. M.; Schöffl, F. Heat stress-induced H(2)O (2) is required for effective expression of heat shock genes in Arabidopsis. *Plant Mol. Biol.* **2006**, *61* (4−5), 733−746.

(6) Guihur, A.; Rebeaud, M. E.; Goloubinoff, P. How do plants feel the heat and survive? *Trends Biochem. Sci.* **2022**, *47* (10), 824−838.

(7) Larkindale, J.; Vierling, E. Core genome responses involved in acclimation to high temperature. *Plant Physiol.* **2008**, *146* (2), 748−761.

(8) Mogk, A.; Bukau, B. Role of sHsps in organizing cytosolic protein aggregation and disaggregation. *Cell Stress Chaperones* **2017**, *22* (4), 493−502.

(9) Wang, T. Y.; Wu, J. R.; Duong, N. K. T.; Lu, C. A.; Yeh, C. H.; Wu, S. J. HSP70−4 and farnesylated AtJ3 constitute a specific HSP70/HSP40-based chaperone machinery essential for prolonged heat stress tolerance in Arabidopsis. *J. Plant Physiol.* **2021**, *261*, No. 153430.

(10) Yamada, K.; Fukao, Y.; Hayashi, M.; Fukazawa, M.; Suzuki, I.; Nishimura, M. Cytosolic HSP90 regulates the heat shock response that is responsible for heat acclimation in Arabidopsis thaliana. *J. Biol. Chem.* **2007**, *282* (52), 37794−37804.

(11) Meiri, D.; Tazat, K.; Cohen-Peer, R.; Farchi-Pisanty, O.; Aviezer-Hagai, K.; Avni, A.; Breiman, A. Involvement of Arabidopsis ROF2 (FKBP65) in thermotolerance. *Plant Mol. Biol.* **2010**, *72* (1−2), 191−203.

(12) Ikeda, M.; Mitsuda, N.; Ohme-Takagi, M. Arabidopsis HsfB1 and HsfB2b act as repressors of the expression of heat-inducible Hsfs but positively regulate the acquired thermotolerance. *Plant Physiol.* **2011**, *157* (3), 1243−1254.

(13) Yoshida, T.; Ohama, N.; Nakajima, J.; Kidokoro, S.; Mizoi, J.; Nakashima, K.; Maruyama, K.; Kim, J. M.; Seki, M.; Todaka, D.; et al. Arabidopsis HsfA1 transcription factors function as the main positive regulators in heat shock-responsive gene expression. *Mol. Genet Genomics* **2011**, *286* (5−6), 321−332.

(14) (a) Charng, Y. Y.; Liu, H. C.; Liu, N. Y.; Chi, W. T.; Wang, C. N.; Chang, S. H.; Wang, T. T. A heat-inducible transcription factor, HsfA2, is required for extension of acquired thermotolerance in Arabidopsis. *Plant Physiol.* **2007**, *143* (1), 251−262. (b) Schramm, F.; Larkindale, J.; Kiehlmann, E.; Ganguli, A.; Englich, G.; Vierling, E.; von Koskull-Döring, P. A cascade of transcription factor DREB2A and heat stress transcription factor HsfA3 regulates the heat stress response of Arabidopsis. *Plant J.* **2008**, *53* (2), 264−274.

(15) Liu, H. C.; Charng, Y. Y. Common and distinct functions of Arabidopsis class A1 and A2 heat shock factors in diverse abiotic stress responses and development. *Plant Physiol.* **2013**, *163* (1), 276−290.

(16) Yoshida, T.; Sakuma, Y.; Todaka, D.; Maruyama, K.; Qin, F.; Mizoi, J.; Kidokoro, S.; Fujita, Y.; Shinozaki, K.; Yamaguchi-Shinozaki, K. Functional analysis of an Arabidopsis heat-shock transcription factor HsfA3 in the transcriptional cascade downstream of the DREB2A stress-regulatory system. *Biochem. Biophys. Res. Commun.* **2008**, *368* (3), 515−521.

(17) Hwang, S. M.; Kim, D. W.; Woo, M. S.; Jeong, H. S.; Son, Y. S.; Akhter, S.; Choi, G. J.; Bahk, J. D. Functional characterization of Arabidopsis HsfA6a as a heat-shock transcription factor under high salinity and dehydration conditions. *Plant, Cell Environ.* **2014**, *37* (5), 1202−1222.

(18) Driedonks, N.; Xu, J.; Peters, J. L.; Park, S.; Rieu, I. Multi-Level Interactions Between Heat Shock Factors, Heat Shock Proteins, and the Redox System Regulate Acclimation to Heat. *Front Plant Sci.* **2015**, *6*, 999.

(19) Pérez-Salamó, I.; Papdi, C.; Rigó, G.; Zsigmond, L.; Vilela, B.; Lumbreras, V.; Nagy, I.; Horváth, B.; Domoki, M.; Darula, Z.; et al. The heat shock factor A4A confers salt tolerance and is regulated by oxidative stress and the mitogen-activated protein kinases MPK3 and MPK6. *Plant Physiol.* **2014**, *165* (1), 319−334.

(20) Evrard, A.; Kumar, M.; Lecourieux, D.; Lucks, J.; von Koskull-Döring, P.; Hirt, H. Regulation of the heat stress response in Arabidopsis by MPK6-targeted phosphorylation of the heat stress factor HsfA2. *PeerJ* **2013**, *1*, No. e59.

(21) Cohen-Peer, R.; Schuster, S.; Meiri, D.; Breiman, A.; Avni, A. Sumoylation of Arabidopsis heat shock factor A2 (HsfA2) modifies its activity during acquired thermotolerance. *Plant Mol. Biol.* **2010**, *74* (1−2), 33−45.

(22) Liu, Y.; Zhang, C.; Chen, J.; Guo, L.; Li, X.; Li, W.; Yu, Z.; Deng, J.; Zhang, P.; Zhang, K.; Zhang, L. Arabidopsis heat shock factor HsfA1a directly senses heat stress, pH changes, and hydrogen peroxide via the engagement of redox state. *Plant Physiol. Biochem.* **2013**, *64*, 92−98.

(23) Chan-Schaminet, K. Y.; Baniwal, S. K.; Bublak, D.; Nover, L.; Scharf, K. D. Specific interaction between tomato HsfA1 and HsfA2 creates hetero-oligomeric superactivator complexes for synergistic activation of heat stress gene expression. *J. Biol. Chem.* **2009**, *284* (31), 20848−20857.

(24) Hahn, A.; Bublak, D.; Schleiff, E.; Scharf, K. D. Crosstalk between Hsp90 and Hsp70 chaperones and heat stress transcription factors in tomato. *Plant Cell* **2011**, *23* (2), 741−755.

(25) Neudegger, T.; Verghese, J.; Hayer-Hartl, M.; Hartl, F. U.; Bracher, A. Structure of human heat-shock transcription factor 1 in complex with DNA. *Nat. Struct. Mol. Biol.* **2016**, *23* (2), 140−146.

(26) Qin, F.; Sakuma, Y.; Tran, L. S.; Maruyama, K.; Kidokoro, S.; Fujita, Y.; Fujita, M.; Umezawa, T.; Sawano, Y.; Miyazono, K.; et al. Arabidopsis DREB2A-interacting proteins function as RING E3 ligases and negatively regulate plant drought stress-responsive gene expression. *Plant Cell* **2008**, *20* (6), 1693−1707.

(27) Niu, W. T.; Han, X. W.; Wei, S. S.; Shang, Z. L.; Wang, J.; Yang, D. W.; Fan, X.; Gao, F.; Zheng, S. Z.; Bai, J. T.; et al. Arabidopsis cyclic nucleotide-gated channel 6 is negatively modulated by multiple calmodulin isoforms during heat shock. *J. Exp. Bot.* **2020**, *71* (1), 90−104.

(28) Ohama, N.; Kusakabe, K.; Mizoi, J.; Zhao, H.; Kidokoro, S.; Koizumi, S.; Takahashi, F.; Ishida, T.; Yanagisawa, S.; Shinozaki, K.; Yamaguchi-Shinozaki, K. The Transcriptional Cascade in the Heat Stress Response of Arabidopsis Is Strictly Regulated at the Level of Transcription Factor Expression. *Plant Cell* **2016**, *28* (1), 181−201.

(29) Guo, M.; Liu, J. H.; Ma, X.; Luo, D. X.; Gong, Z. H.; Lu, M. H. The Plant Heat Stress Transcription Factors (HSFs): Structure, Regulation, and Function in Response to Abiotic Stresses. *Front. Plant Sci.* **2016**, *7*, 114.

(30) Aviezer-Hagai, K.; Skovorodnikova, J.; Galigniana, M.; Farchi-Pisanty, O.; Maayan, E.; Bocovza, S.; Efrat, Y.; von Koskull-Döring, P.; Ohad, N.; Breiman, A. Arabidopsis immunophilins ROF1 (AtFKBP62) and ROF2 (AtFKBP65) exhibit tissue specificity, are heat-stress induced, and bind HSP90. *Plant Mol. Biol.* **2007**, *63* (2), 237−255.

(31) Meiri, D.; Breiman, A. Arabidopsis ROF1 (FKBP62) modulates thermotolerance by interacting with HSP90.1 and affecting the accumulation of HsfA2-regulated sHSPs. *Plant J.* **2009**, *59* (3), 387−399.

(32) Oxley, D.; Ktistakis, N.; Farmaki, T. Differential isolation and identification of PI(3)P and PI(3,5)P2 binding proteins from Arabidopsis thaliana using an agarose-phosphatidylinositol-phosphate affinity chromatography. *J. Proteomics* **2013**, *91*, 580−594.

(33) Karali, D.; Oxley, D.; Runions, J.; Ktistakis, N.; Farmaki, T. The Arabidopsis thaliana immunophilin ROF1 directly interacts with PI(3)P and PI(3,5)P2 and affects germination under osmotic stress. *PLoS One* **2012**, *7* (11), No. e48241.

(34) Thirumalaikumar, V. P.; Gorka, M.; Schulz, K.; Masclaux-Daubresse, C.; Sampathkumar, A.; Skirycz, A.; Vierstra, R. D.;

https://doi.org/10.1021/acsomega.3c06773
ACS Omega 2024, 9, 2391−2408

Balazadeh, S. Selective autophagy regulates heat stress memory in Arabidopsis by NBR1-mediated targeting of HSP90.1 and ROF1. *Autophagy* **2021**, *17* (9), 2184−2199.
(35) Maniatsi, S.; Farmaki, T.; Abatzopoulos, T. J. The study of fkbp and ubiquitin reveals interesting aspects of Artemia stress history. *Comp. Biochem. Physiol., Part B: Biochem. Mol. Biol.* **2015**, *186*, 8−19.
(36) Perez-Riverol, Y.; Bai, J.; Bandla, C.; García-Seisdedos, D.; Hewapathirana, S.; Kamatchinathan, S.; Kundu, D. J.; Prakash, A.; Frericks-Zipper, A.; Eisenacher, M.; et al. The PRIDE database resources in 2022: a hub for mass spectrometry-based proteomics evidences. *Nucleic Acids Res.* **2022**, *50* (D1), D543−D552.
(37) Zhou, Y.; Zhou, B.; Pache, L.; Chang, M.; Khodabakhshi, A. H.; Tanaseichuk, O.; Benner, C.; Chanda, S. K. Metascape provides a biologist-oriented resource for the analysis of systems-level datasets. *Nat. Commun.* **2019**, *10* (1), No. 1523.
(38) Kurek, I.; Stöger, E.; Dulberger, R.; Christou, P.; Breiman, A. Overexpression of the wheat FK506-binding protein 73 (FKBP73) and the heat-induced wheat FKBP77 in transgenic wheat reveals different functions of the two isoforms. *Transgenic Res.* **2002**, *11* (4), 373−379.
(39) Kurek, I.; Aviezer, K.; Erel, N.; Herman, E.; Breiman, A. The wheat peptidyl prolyl cis-trans-isomerase FKBP77 is heat induced and developmentally regulated. *Plant Physiol.* **1999**, *119* (2), 693−704.
(40) Reddy, R. K.; Kurek, I.; Silverstein, A. M.; Chinkers, M.; Breiman, A.; Krishna, P. High-molecular-weight FK506-binding proteins are components of heat-shock protein 90 heterocomplexes in wheat germ lysate. *Plant Physiol.* **1998**, *118* (4), 1395−1401.
(41) Li, J.; Soroka, J.; Buchner, J. The Hsp90 chaperone machinery: conformational dynamics and regulation by co-chaperones. *Biochim. Biophys. Acta, Mol. Cell Res.* **2012**, *1823* (3), 624−635.
(42) Fernández-Bautista, N.; Fernández-Calvino, L.; Muñoz, A.; Toribio, R.; Mock, H. P.; Castellano, M. M. HOP family plays a major role in long-term acquired thermotolerance in Arabidopsis. *Plant, Cell Environ.* **2018**, *41* (8), 1852−1869.
(43) Prodromou, C.; Panaretou, B.; Chohan, S.; Siligardi, G.; O'Brien, R.; Ladbury, J. E.; Roe, S. M.; Piper, P. W.; Pearl, L. H. The ATPase cycle of Hsp90 drives a molecular 'clamp' via transient dimerization of the N-terminal domains. *EMBO J.* **2000**, *19* (16), 4383−4392.
(44) Hessling, M.; Richter, K.; Buchner, J. Dissection of the ATP-induced conformational cycle of the molecular chaperone Hsp90. *Nat. Struct. Mol. Biol.* **2009**, *16* (3), 287−293.
(45) Mayer, M. P. Hsp70 chaperone dynamics and molecular mechanism. *Trends Biochem. Sci.* **2013**, *38* (10), 507−514.
(46) Fu, C.; Hou, Y.; Ge, J.; Zhang, L.; Liu, X.; Huo, P.; Liu, J. Increased fes1a thermotolerance is induced by BAG6 knockout. *Plant Mol. Biol.* **2019**, *100* (1−2), 73−82.
(47) Zhang, W.; Zhou, R. G.; Gao, Y. J.; Zheng, S. Z.; Xu, P.; Zhang, S. Q.; Sun, D. Y. Molecular and genetic evidence for the key role of AtCaM3 in heat-shock signal transduction in Arabidopsis. *Plant Physiol.* **2009**, *149* (4), 1773−1784.
(48) Buchberger, A. Roles of Cdc48 in regulated protein degradation in yeast. *Subcell. Biochem.* **2013**, *66*, 195−222.
(49) Fishbain, S.; Prakash, S.; Herrig, A.; Elsasser, S.; Matouschek, A. Rad23 escapes degradation because it lacks a proteasome initiation region. *Nat. Commun.* **2011**, *2*, No. 192.
(50) Wade, S. L.; Auble, D. T. The Rad23 ubiquitin receptor, the proteasome and functional specificity in transcriptional control. *Transcription* **2010**, *1* (1), 22−26.
(51) Kawazoe, Y.; Nakai, A.; Tanabe, M.; Nagata, K. Proteasome inhibition leads to the activation of all members of the heat-shock-factor family. *Eur. J. Biochem.* **1998**, *255* (2), 356−362.
(52) Peterman, T. K.; Ohol, Y. M.; McReynolds, L. J.; Luna, E. J. Patellin1, a novel Sec14-like protein, localizes to the cell plate and binds phosphoinositides. *Plant Physiol.* **2004**, *136* (2), 3080−3094.

https://doi.org/10.1021/acsomega.3c06773
ACS Omega 2024, 9, 2391−2408